Multiple episodes of gold mineralization in the East Kunlun Orogen, western Central Orogenic Belt, China: Constraints from Re-Os sulfide geochronology

Jiajie Chen[1,2,3]· Lebing Fu[2] ·David Selby[3] ·Junhao Wei[2] ·Xu Zhao[2] ·Hongzhi Zhou[2]

[1] State Key Laboratory of Nuclear Resources and Environment, School of Earth Sciences, East China University of Technology, Nanchang, 330013, China

[2] Faculty of Earth Resources, China University of Geosciences, Wuhan, 430074, China

[3] Department of Earth Sciences, University of Durham, Durham, DH1 3LE, UK

✉ Junhao Wei

E-mail: junhaow@163.com

Tel: +86-13437179812.

Abstract

The Gouli goldfield (>110 t Au), located in the East Kunlun Orogen, western Central Orogenic Belt of China, is one of the most important goldfields in this area. In the last decade, a number of orogenic gold deposits (e.g., Guoluolongwa and Annage) have been shown to be hosted by rock units of different lithology and ages. Rhenium-osmium (Re-Os) geochronology of sulfides from gold-bearing veins was performed to define the chronologic relationships between gold mineralization present in the metamorphic rocks (Proterozoic and Silurian) of the East Kunlun Orogen. Sulfides (pyrite and chalcopyrite) from pyrite-quartz vein and polymetallic sulfides-quartz vein in the Guoluolongwa gold deposit yield Re-Os isochron dates of 374 ± 15 Ma (MSWD = 4.6; initial $^{187}Os/^{188}Os$ ratio (Osi) = 0.06 ± 0.22) and 354 ± 7 Ma (MSWD = 0.18; Osi = 0.13 ± 0.01), respectively. Similar ages are also revealed by the pyrite mineral separates from the Annage gold deposit (383 ± 8 Ma and 349 ± 6 Ma). These ages are interpreted to record the timings of the formation of the two vein types in these deposits, which are nominally separated by ~20 Ma.

The new Re-Os ages presented here identify the first two Late Paleozoic (Devonian and Early Carboniferous) gold-mineralizing events in the East Kunlun Orogen and thus indicate at least two mineralization epochs in this area given ages (Late Triassic) of other gold systems and field observations. Considering the geological background and temporal distribution of gold deposits in adjacent areas (western Qinling and Qaidam-Qilian), we suggest that gold deposits in the western Central Orogenic Belt were formed in collisional/post-collisional settings being controlled by common tectonic-magmatic activities

related to the evolution of both the Prototethys Ocean (Proterozoic – Paleozoic) and Paleotethys Ocean (Paleozoic – Early Cenozoic).

Further, the initial Os (Osi) obtained from the Re-Os isochron suggest that for the two vein types in the Guoluolongwa gold deposit the Os and by inference the ore metal (Au) were derived from a mantle-like source (Osi values = ~0.12 – 0.13), which should be related to the contemporaneous mantle-like magmatism. In contrast, the pyrite-quartz vein in the Annage gold deposit possesses a significantly radiogenic Osi value (3.65 ± 0.51). Given the similar timing of mineralization between the Guoluolongwa and Annage deposits, it is considered that the ore metal likely has a similar origin, i.e., a mantle-like source, however at Annage the hydrothermal fluid interacted with the Proterozoic metamorphic host rocks and leached radiogenic Os that masks any evidence of a mantle-like source.

Keywords: Gold deposit; Paleozoic mineralization; Re-Os isotopic dating; East Kunlun Orogen

1. Introduction

The East Kunlun Orogen, comprising the western part of the Central Orogenic Belt of China (Fig. 1A), records two stages of orogenesis that correspond to the evolution of the Neoproterozoic–Late Paleozoic Prototethys Ocean and Late Paleozoic–Triassic Paleotethys Ocean in this area (Fig. 1B; Ma et al., 2015). During the last ten years, in the East Kunlun Orogen, a number of gold deposits/fields, such as the Wulonggou (>70 t Au; unpublished report; Zhang et al., 2017) and Gouli (>110 t Au; unpublished report) goldfields, and the Balong and Kaihuangbei gold deposits, have been discovered (Fig.1C; Zhao, 2004 and references therein). Most of the gold deposits/fields exhibit quartz-vein type or fracture-hosted pervasive alteration type mineralization and are spatially controlled by brittle-ductile shear zones and, in turn, have been regarded to be orogenic gold deposits (Feng, 2002; Zhao, 2004). A Silurian–Devonian timing, coincident with that of the evolution of Prototethys, has been proposed to be responsible for the formation of these deposits based on the conclusion that the ore-controlling structures were formed during the Silurian-Devonian tectonic deformation (e.g., Zhang et al., 2001; Feng, 2002 and references therein). However, reported Ar-Ar dating of sericite or muscovite from gold deposits in the East Kunlun Orogen revealed a Triassic age population (Feng, 2002; Zhao, 2004; Zhang et al., 2005; Xiao et al., 2014; Zhang et al., 2017). This, together with the close spatial relationship between some gold deposits and ubiquitous Late Permian-Triassic granitoids (Li et al., 2012; Zhang et al., 2017) is taken to suggest that the Triassic gold-mineralizing dominated the formation of these deposits, although the gold deposits in this area are hosted by different geological units of

various ages (from Paleozoic to Mesozoic). The lack of a temporal record of Paleozoic "gold mineralization" may be due to: (1) an early Paleozoic mineralization event did not occur, and (2) post-ore thermal events, such as Triassic mineralization or extensive magmatism, have reset the Ar-Ar systems in micaceous minerals due to the susceptibility of this system to hydrothermal overprint (Selby et al., 2002). The ambiguity of the timing of the early and late "gold-mineralizing events" not only hampers our understanding of the origin of these gold deposits but also exploration. As such, a more robust dating method is required.

Recently, rhenium-osmium (Re-Os) isotopic dating of sulfide minerals (e.g., pyrite, chalcopyrite, and molybdenite) has been applied to several types of hydrothermal deposits. Among these sulfide minerals, molybdenite is particularly suitable for Re-Os geochronology, given its high abundance of Re (typically ppm levels) and negligible common Os (Stein et al., 2003; Selby and Creaser, 2004). However, molybdenite is commonly absent in many gold deposits, nevertheless other sulfides, e.g. pyrite (Stein et al., 2000), arsenopyrite (Morelli et al., 2005; Morelli et al., 2007), chalcopyrite (Lawley et al., 2013), bornite (Selby et al., 2009) and even pyrrhotite (Wang et al., 2008) can be utilized to delineate the timing of gold mineralization. In this contribution, we present Re-Os geochronology on gold-related pyrite and chalcopyrite from two deposits in the Gouli goldfield located in the eastern East Kunlun Orogen, western Central Orogenic Belt to pinpoint the timing of gold mineralization and constrain the sources of ore-forming materials. We demonstrate that at least two gold mineralizing epochs (Late Paleozoic and Late Triassic) exist in the East Kunlun Orogen and

possibly wider west of Central Orogenic Belt and that the ore metal (Au) exhibit a mantle-like derived origin.

2. Regional and deposit geology

The East Kunlun Orogen is located in the northern Tibet and is bounded by the Qaidam Basin to the north, the Qinling Orogen to the east, the Bayan Har Terrane to the south and the Altyn Tagh fault to the west (Fig. 1B). The East Kunlun Orogen is composed of the Northern East Kunlun Terrane and the Southern East Kunlun Terrane, which are separated by the Central East Kunlun Suture Zone (Fig. 1C). Two regional suture zones, the Central East Kunlun Suture Zone and Southern East Kunlun Suture Zone, which correspond to the evolution of the Prototethys Ocean (Proterozoic–Early Paleozoic) and Paleotethys Ocean (Late Paleozoic – Mesozoic), respectively, traverse the East Kunlun Orogen (e.g., Yang et al., 1996). The basement rocks in the East Kunlun Orogen are composed of Proterozoic intermediate – high - grade metamorphic rocks that are mainly exposed in the Northern East Kunlun Terrane (Meng et al., 2013; He et al., 2016; Wei et al., 2016). Overlying these basement rocks are the Early Paleozoic low-grade metamorphic sedimentary and volcanic rocks (e.g., Chen et al., 2013; Chen et al., 2014) that are unconformably overlain by the Devonian Maoniushan Formation (molasse) (e.g., Zhang et al., 2010). Carboniferous–Middle Triassic marine facies rocks mainly occur in the Southern East Kunlun Terrane. Magmatic rocks in the East Kunlun Orogen consist of granitoids with minor mafic-ultramafic rocks (Fig. 1C). The mafic-ultramafic rocks occur mainly along the Central East Kunlun Suture Zone and Southern East Kunlun Suture Zone. The mafic-ultramafic rocks from the Central East Kunlun Suture Zone

are dated as Cambrian-Ordovician with ages that range from 537 Ma to 467 Ma (Zhu et al., 2000; Bian et al., 2004; Li et al., 2013; Wei, 2015; Qi et al., 2016). The mafic-ultramafic units from the Southern East Kunlun Suture Zone exhibit both Cambrian-Ordovician (555–516 Ma; Li, 2008; Liu et al., 2011) and Carboniferous ages (345–332 Ma; Chen et al., 2001; Liu et al., 2011). The granitoids yield dates mainly concentrated in Ordovician-Devonian (470–390 Ma) and Permian-Triassic (260–220 Ma) (Mo et al., 2007). Granitoids in both age groups show time-varying lithology from early calc-alkaline granodiorites to late monzogranites and syenogranites (e.g., Lu et al., 2013; Zhang et al., 2014; Chen et al., 2016; Chen et al., 2017). Succeeding the Ordovician-Devonian massive intrusion of granitoids were widespread volcanic activities, which are evidenced by bimodal volcanic rocks from the Maoniushan Formation (Zhang et al., 2010; Liu et al., 2016).

2.1 Geology of the Gouli goldfield

The Gouli goldfield is located in the east end of the East Kunlun Orogen (Fig. 1C). The Central East Kunlun Suture Zone, which is evidenced by the ophiolites, traverses the central part of this area (Fig. 2). Proterozoic middle–high-grade metamorphic basement rocks occur across the entire area. Overlying the basement rocks are the Ordovician-Silurian low-grade metamorphic rocks from the Naij Tai Group, Devonian Maoniushan Formation and the Carboniferous–Triassic sedimentary and volcanic rocks. The lithology of magmatic rocks varies from mafic-ultramafic intrusions/dikes to felsic granitoids. The mafic-ultramafic rocks exhibit Cambrian and Devonian-Carboniferous ages (Yang et al., 1996; Chen et al., 2001; Feng et al., 2010), with the felsic granitoids mainly defining two age groups, Ordovician-

Devonian and Permian-Triassic (Fig. 2). A number of gold deposits have been discovered in this field, including the Guoluolongwa (>40 t Au), Annage (>8 t Au), Asiha (>6 t Au), Walega (>12 t Au) and Delong (>5 t Au) (unpublished report). These deposits can be divided into two groups according to their host rocks, ore-controlling structure, mineralization styles, and alteration. Group one, represented by the Guoluolongwa and Annage, is hosted in metamorphic rocks (Proterozoic for Annage and Silurian for Guoluolongwa) (Figs 2–4; Ding et al., 2013; Tao, 2014), mainly controlled by EW-trending brittle-ductile shear zone, which contrast to the Group two deposits (represented by the Walega and Asiha) being hosted in Silurian (Fig. 2; 431–440 Ma; our unpublished data) or Triassic (238–244 Ma; Fig. 2; Li et al., 2012; Li et al., 2014) felsic intrusions and mainly controlled by NW or NE-trending brittle fractures (Chen, 2018) . The gold mineralization of both groups is mainly associated with quartz veins and subordinate associated with pervasively altered fracture zones. However, the mineral assemblages of the two groups are distinct, with group one showing sulfides dominated by pyrite and those of group two dominated by arsenopyrite (Chen, 2018). The close spatial relationship of these deposits makes researchers consider that these deposits were formed by a common mineralization event during Triassic after the emplacement of the youngest host (Asiha quartz diorite) (Yue, 2013).

2.2 Geology of the Guoluolongwa and Annage gold deposits

In the Central East Kunlun Suture Zone, the Guoluolongwa gold deposit is the largest gold deposit in the Gouli goldfield. The ore deposit is structurally controlled by the Silurian–Devonian formed (427–408 Ma; Wang et al., 2003), EW-trending thrust zone. In the north of

the deposit is the oldest rock unit, Proterozoic aged schist (Fig. 3). In the center of the deposit are the Ordovician-Silurian Naij Tal Group metamorphic rocks, which have zircon U-Pb ages of 479.1 ± 2.4 and 479.7 ± 5.6 Ma, indicating that the sedimentary and volcanic protoliths were formed no later than 479 Ma. (Fig. 3A; our unpublished data). In the south of the deposit are conglomerates of the Devonian Maoniushan Formation (e.g., Lu et al., 2010). Magmatic rocks in this area include mylonitic diorite (~ 477 Ma; our unpublished data) and gabbro (416 Ma; Yue et al., 2013).

Six gold orebodies (I – VI) have been delineated in the Guoluolongwa gold system (Fig. 3). All of the orebodies show an EW trend (Fig. 3A) and high angle dips (50 – 80°) towards the south (180°; Fig. 3B). The gold grades vary from 1 g/t to hundreds g/t, with an average grade at 6.75 g/t (Fig. 3B; unpublished geological report). The gold mineralization is mainly associated with quartz veins that cross cut the Devonian gabbro (Yue et al., 2013), with subordinate pervasively altered fracture-hosted mineralization occurring in the north of the deposit area (Xiao et al., 2014).

Three stages of mineralization are defined at the Guoluolongwa based on mineral assemblages and crosscutting relationships (Figs. 5–6). The first stage is characterized by coarse milky quartz with sparse coarse pyrite (up to 5 mm) (stage I vein), which is cross-cut by the disseminated-massive pyrite-quartz vein of the second stage (stage II vein). Both coarse and fine grain pyrite can be observed in the stage II vein (Fig. 5H) that are cut cross by the polymetallic stage III quartz vein (Figs. 5D and H). Minerals in the stage III quartz vein mainly include pyrite, sphalerite, galena, chalcopyrite and quartz (Figs. 5D and I).

Native gold can be found in fractures of pyrite and between grains of sulfide and quartz (Figs. 5D and E) or as inclusions enwrapped in pyrite and quartz (Yang et al., 2006). High-grade gold ores are found associated with both stage Ⅱ and Ⅲ veins.

The Annage gold deposit is located to the immediate northwest (<3km) of the Guoluolongwa deposit (Fig. 2). As such the local geology is very similar to that of the Guoluolongwa deposit. But in contrast, the ore bodies are hosted by Proterozoic metamorphic mica-quartz schist, amphibolite and marble units (Fig. 4). Most of the Annage orebodies (I, Ⅱ, Ⅴ, and Ⅵ; Fig. 4) strike east-west and dip 50 – 85° to south-southwest (Fig. 4). The orebodies as a whole show identical mineralization stages and mineral assemblages to those of the Guoluolongwa system (Chen, 2014; Tao, 2014), suggesting that the two gold deposits should have a common origin. However, some orebodies at Annage (e.g., orebody I; Figs. 4 and 5J-I) are dominated by stage Ⅱ vein (gold grade averaging at 5.18 g/t) with the stage Ⅲ polymetallic sulfides-quartz vein mineralization poorly developed. The ore grades vary widely (grades of different ore bodies average between 1.06 and 43.51 g/t), with the highest grade being 156 g/t.

3. Sampling and analytical methods

To define the timing of sulfide (± gold) mineralization by application of the Re-Os chronometer, fourteen samples from the quartz vein orebodies (seven from the stage Ⅱ veins and seven from the stage Ⅲ veins) of the Guoluolongwa system and 10 samples from the pyrite-quartz veins (orebody I; Fig. 5E) of the Annage gold deposit were selected. For the Guoluolongwa system, samples are all collected from the underground tunnel of orebodies I

and Ⅵ (Fig. 3). Samples for the stage Ⅱ quartz veins were collected from the massive or veinlet ores (Figs. 5A and B), both of which crosscut the stage I milky quartz veins. Samples for the stage Ⅲ quartz veins were collected from dense disseminated ores that are mainly composed of galena, sphalerite, chalcopyrite, pyrite and quartz (Fig. 5C). In total, seven pyrite mineral separates from the stage Ⅱ veins, and four pyrite and three chalcopyrite mineral separates from the stage Ⅲ veins were prepared for the Guoluolongwa gold deposit. For the Annage deposit, the samples were all collected from the open mining pit of orebody I (Fig. 4) that is mainly composed of Stage Ⅱ pyrite-quartz vein (Figs. 5J and K). In total, ten pyrite mineral separates were prepared. The mineral separates were obtained using traditional isolation methods (e.g., crushing, heavy liquids separation and handpicking).

The Re-Os analyses were conducted at the Source Rock and Sulfide Geochronology and Geochemistry Laboratory at Durham University. The analytical method is described below. The purified mineral separate of about 400 mg was accurately weighed and loaded into a Carius tube with a known amount of mixed Re-Os tracer solution containing ^{185}Re and ^{190}Os, and a mixture of 11 *N* HCl (3 ml) and 15.5 *N* HNO_3 (6 ml) (inverse aqua regia). The Carius tube was sealed and then placed into an oven at 220 ^{o}C for 24 h to permit sample and tracer digestion and equilibration. Osmium was isolated from the inverse aqua regia using solvent extraction ($CHCl_3$) method and purified by microdistillation, and rhenium was isolated using solvent extraction (NaOH-acetone) followed by anion column chromatography methods (Selby et al., 2009; Cumming et al., 2013). The purified Re and Os were loaded onto outgassed Ni and Pt filaments with corresponding activators (barium nitrate and sodium-

barium hydroxide), respectively (Selby et al., 2009). The Re and Os isotope compositions were measured using negative thermal ionization mass spectrometry on a Thermo Scientific TRITON mass spectrometer using static Faraday collection for Re and secondary electron multiplier in peak–hopping mode for Os. Total procedural blanks of this study for Re and Os were 2.3 +/- 0.2 and 0.08 +/- 0.02 pg, with an average $^{187}Os/^{188}Os$ value of 0.25 ± 0.05 (n = 3). All uncertainties are calculated by error propagation of uncertainties in Re and Os mass spectrometer measurements, blank abundances and isotopic compositions, spike calibrations, sample and spike weights, and reproducibility of standard Re and Os isotope values. The operational conditions of the mass spectrometer were monitored by solution reference materials which yielded values of 0.16087 ± 0.00026 for DROsS and 0.5993 ± 0.0006 (1SD, n=9) for the Re standard. These values are in agreement with those reported previously (e.g., Selby, 2007; Nowell et al., 2008). The Re-Os isochron age, ^{187}Re-$^{187}Os^{r}$ isochron age, and weighted mean age were determined using Isoplot/Ex_version 3.75 (Ludwig, 2012).

4. Results

The Re-Os data are presented in Table 1 and Figures 7 – 10. The Re and Os abundances in the pyrite from the stage II vein in the Guoluolongwa gold deposit varies widely, from 0.06 to 0.57 ppb and 1.5 to 228.8 ppt, respectively. The $^{187}Re/^{188}Os$ (4.57 – 4917.48) and $^{187}Os/^{188}Os$ (0.15 – 31.19) ratios display highly variable values and yield a Re-Os isochron Model 3 date of 374 ± 15 Ma (MSWD = 4.6) and initial $^{187}Os/^{188}Os$ (Osi) of 0.06 ± 0.22. Using the Osi value from the isochron, with the exception of Au4-1, the sample set possesses ≥ 93 % radiogenic ^{187}Os ($^{187}Os^{r}$) and are therefore characterized as low level highly

radiogenic sulfides (LLHR, Stein et al., 2000) . In contrast, sample Au4-1 exhibits a high abundance of common Os (^{192}Os = 94.2 ppt). Individually, the six LLHR samples yield Re-Os model dates of 353 – 394 Ma (Table 1 and Fig. 7C), with a weighted mean age of 375 ± 11 Ma (MSWD = 0.60; Fig. 7C) and ^{187}Re-^{187}Os^{r} isochron date of 373 ± 17 Ma (Fig. 7B; MSWD = 0.68; initial ^{187}Os^{r} = 0.01 ± 0.05). For the sample Au4-1, calculation of model age using the Osi from the isochron yields a highly imprecise and inaccurate date (1147 ± 5724 Ma; Table 1). Further, the weighted average (375 ± 11 Ma; MSWD = 0.51) and ^{187}Re-^{187}Os^{r} isochron date (373 ±17 Ma; MSWD = 0.56; initial ^{187}Os^{r} = 0.01 ± 0.06) is not appreciably affected including data of the sample Au4-1.

Using a date of 375 Ma, the six LLHR samples yield either positive or negative Osi values with significant uncertainties (Table 1), with the non-radiogenic sample, Au4-1, yielding an Osi value of 0.12 ± 0.01 (Table 1 and Fig. 10). Based on this Osi value, model dates for all samples are recalculated, which yield a weighted mean date of 365 ± 16 Ma (all samples; MSWD = 3.70; Fig. 7C) and 365 ± 19 Ma (excluding sample Au4-1; MSWD = 4.4; Fig. 7C).

The Re and Os abundances in pyrite from the stage III vein of the Guoluolongwa gold deposit are 0.17 – 0.62 ppb and 1.4 – 3.7 ppt, respectively. The chalcopyrite mineral separates display much lower Re abundances (0.01 –0.06 ppb) and wide range of Os contents (0.8 – 322.2 ppt). As a whole, the ^{187}Re/^{188}Os (0.24 – 2809.52) and ^{187}Os/^{188}Os (0.13 – 16.91) data from the four pyrites and the three chalcopyrites yield a Model 1 Re-Os isochron date of 354 ± 7 Ma (MSWD = 0.18; Fig. 8A), with non-radiogenic Osi value of 0.13 ± 0.01. Based on the Osi value defined by the Re-Os isochron, five samples possess > 93% ^{187}Os^{r} and two

samples show a high abundance of common Os (^{192}Os = 16.5 and 132.9 ppt). Individually, the LLHR samples yield Re-Os model dates between 349 and 407 Ma, with the two non-radiogenic samples possessing large uncertainties (Table 1 and Fig. 8C). The ^{187}Re-^{187}Os^{r} isochron date based on the five LLHR samples (355 ± 11 Ma; MSWD = 0.16; initial ^{187}Os^{r} = 0.00 ± 0.02; Fig. 7B) and all samples (355 ± 11 Ma; MSWD = 0.10; initial ^{187}Os^{r} = 0.00 ± 0.01; Fig. 7B), are identical and so are the weighted mean dates (354 ± 7 Ma; Fig. 7C). The Osi values of individual samples calculated based on the weighted mean date vary from 0.05 to 0.32, with the LLHR samples showing significant uncertainties. (Table 1 and Fig. 10)

The Re and Os abundances of pyrite from the Stage II quartz vein of the Annage gold deposit range from 2.4 to 7.6 ppb and 21.9 to 105.1 ppt, respectively (Table 1). The ^{187}Re/^{188}Os (299.13 – 28139.20) and ^{187}Os/^{188}Os (5.53 – 145.66) ratios vary greatly and yield a Re-Os isochron date of 369 ± 18 Ma (MSWD = 24), with radiogenic Osi value of 3.9 ± 2.4 (Fig. 9A). Discarding the sample CK003 that deviates the isochron, the remaining nine samples yield an isochron date of 382.6 ± 8.0 Ma, with a much more precise Osi value (3.65 ± 0.51) and smaller MSWD (6.6; Fig. 9B), indicating that sample CK003 is the cause of the scatter in the linear regression analysis. Using the Osi value of 3.65 ± 0.51, the Re-Os model dates of the nine samples range from 370 to 460 Ma (Table 1 and Fig. 9D). A ^{187}Re-^{187}Os^{r} isochron date of 396 ± 28 Ma (initial ^{187}Os^{r} = -0.8 ±1.5; MSWD = 0.42) and a weighted mean age of 383 ± 6 Ma (MSWD = 0.57) is determined based on the nine samples. Further, using the Osi value of 3.65 ± 0.51, the outlier sample, CK003, yields a model age of 349 ± 6 Ma that approach the isochron age of stage III veins of the Guoluolongwa gold deposit (Table 1).

5. Discussion

5.1 Evaluation of the Re-Os dates and Osi values

The Re-Os isochron date (Fig. 7A; 375 ± 15 Ma) and the ^{187}Re-$^{187}Os^{r}$ isochron date (Fig. 7B; 373 ± 17 Ma) determined from the stage II veins in the Guoluolongwa gold deposit are identical including uncertainty. The weighted mean of the Re-Os model dates based on the Osi value from the Re-Os isochron (0.06 ± 0.22) is in agreement with the age based on the Osi value calculated for the non-radiogenic sample Au4-1 (0.12 ± 0.01) within uncertainty. However, the Re-Os model dates determined based on an Osi value of 0.12 ± 0.01 are nominally younger than the date obtained from that based on Osi value of 0.06 ± 0.22 (365 vs. 375 Ma; Fig. 7) and show much higher MSWD (3.7 and 4.4 vs. 0.5 and 0.6; Fig. 7C). The reason for this is the greater precision in the model Re-Os dates determined using an Osi value of 0.06 ± 0.22 relative to 0.12 ± 0.01. Regardless, all Re-Os date determinations indicate that stage II mineralization at the Guoluolongwa occurred at ~370 Ma suggesting the interval of mineralization occurred between the Latest Devonian and Earliest Carboniferous.

The Osi value from the Re-Os isochron and the LLHR samples show significant uncertainties (Fig. 7A and Table 1), making the geological significance of these Osi values ambiguous. However, the Re-Os data for the non-radiogenic sample (Au4-1) yields a highly precise Osi value (0.12 ± 0.01). Considering the much higher common Os of this sample (Au4-1) than those for the LLHR samples, the ^{188}Os determination of this sample is more reliable and so is the Osi value (Stein et al., 2000). Consequently, we take 0.12 ± 0.01 to

represent the best estimate of Osi composition of these samples, which is almost identical to Osi values of the stage III vein in the Guoluolongwa gold deposit (discussed below).

The Re-Os isochron date (354 ± 7 Ma), ^{187}Re-$^{187}Os^{r}$ isochron date (355 ± 11 Ma) and weighted mean dates (354 ± 7 Ma) based on all samples from the stage III vein in the Guoluolongwa gold deposit are identical, with the MSWD values corresponding to these dates being < 0.3, indicating that the degree of scattering in the data set is almost entirely analytical. As such the timing of the stage III mineralization is taken to be ~355 Ma (±7 - 11). The Osi values from the Re-Os isochron and the non-radiogenic samples are consistent, at 0.13 ± 0.01, which are taken to represent the best estimate of the Osi composition of the stage III mineralization.

The two Re-Os isochron dates (369 ± 18 Ma (all samples) and 383 ± 8 Ma (excluding sample CK003)) from the stage II quartz veins in the Annage gold deposit are similar including the uncertainty. However, the uncertainty of the age 369 Ma is much larger (18 vs. 8 Ma) and so is the uncertainty in the corresponding Osi (2.4 vs. 0.5) and degree of scatter about the best fit of the data (MSWD = 24 vs. 6.6). The scatter coupled with the obvious deviation of the CK003 from the best fit of all the Re-Os data (Fig. 9A) indicate the CK003 could relate to a different stage of mineralization from that of the stage III mineralization and/or its Re-Os systematics are slightly disturbed. The model Re-Os date for sample CK003 is much younger than those of other samples (349 ± 6 Ma). As such, we regard the Re-Os isochron date determined from all samples with the exception of CK003 (383 ± 8 Ma) as the best estimate of the timing of the stage II veins at Annage. This age is consistent with the

weighted mean date of the Re-Os model dates (383 ± 6 Ma) and within the uncertainty of the ^{187}Re-$^{187}Os^{r}$ isochron date (396 ± 28 Ma). Interestingly, the Re-Os model date of the sample CK003 (349 ± 6 Ma) is consistent with that of stage Ⅲ veins in the Guoluolongwa gold deposit, indicating that a common Carboniferous event may occur in the two deposit. The Osi value from the Re-Os isochron (3.65 ± 0.51) is similar to those calculated for each sample (~2.9 to 4.3 excluding CK003) and could be taken to represent the initial compositions of these samples.

5.2 Multiple gold-mineralizing events in the East Kunlun Orogen

Muscovite collected from the gold-bearing vein in the Guoluolongwa yields a Late Triassic $^{40}Ar/^{39}Ar$ plateau age that was interpreted as the timing of gold mineralization (202.7 ± 1.5 Ma; Xiao et al., 2014). Although, no detailed paragenesis between the muscovite and gold/gold-bearing minerals are reported (Xiao et al., 2014), it is considered that the Guoluolongwa gold deposit, and even all gold deposits in the Gouli goldfield, are Triassic in age, similar to many other gold deposits/fields in the East Kunlun Orogen and adjacent areas, e.g., Wulonggou (sericite Ar-Ar, 236.5 ± 0.5 Ma; Zhang et al., 2005), Shuizhadonggou (deposit in the Wulonggou gold field; sericite Ar-Ar, 237-231 Ma; Zhang et al., 2017) and Dachang (sericite Ar-Ar, 218.6 ±3.2 Ma; Zhang et al., 2005). However, the Re-Os data obtained from directly analyzing of sulfides (pyrite and chalcopyrite) from the Guoluolongwa and Annage yield much older ages (Late Devonian and Early Carboniferous) and thus it is necessary to re-evaluate the Triassic age gained from Ar-Ar dating and timing of gold mineralization of these deposits in the East Kunlun Orogen.

Crosscutting relationships of different geological units can offer the first-order constraint on the timing of the gold mineralizing events. In the Guoluolongwa gold deposit, field observations indicate that the hydrothermal veins related to gold mineralization cut cross the gabbro (416.2 ± 3.5 Ma; Yue et al., 2013) and the stage Ⅱ pyrite-quartz vein are crosscut by the stage Ⅲ polymetallic sulfides-quartz veins (Fig.5 A). Thus, both types of gold-bearing veins should be emplaced after ~416 Ma and the stage Ⅱ pyrite-quartz vein must be older than the stage Ⅲ polymetallic sulfides-quartz vein. These conclusions are consistent with our data (375 ± 11 Ma and 354 ± 7 Ma, respectively), but cannot explain the contradictory results between our Re-Os dates and the previously reported muscovite Ar-Ar age (202.7 ± 1.5 Ma; Xiao et al., 2014). Two possible models are: (1) the Paleozoic ages obtained from the Re-Os data of the sulfides represent the timing of gold mineralization, with the $^{40}Ar/^{39}Ar$ plateau age from muscovite being a product of a late thermal/hydrothermal overprint; (2) the $^{40}Ar/^{39}Ar$ plateau age represent the timing of gold mineralization, while sulfides were contaminated by old rocks during fluid migration leading to inhomogeneous initial $^{187}Os/^{188}Os$ compositions of sulfide samples and thus result in an errorchron or pseudochron (Yang et al., 2008). A valid method to test the two models is to plot initial $^{187}Os/^{188}Os$ against $1/^{192}Os$ (Faure and Mensing, 2005). If model two is correct, a linear relationship between the initial $^{187}Os/^{188}Os$ and $1/^{192}Os$ should be expressed by the data. However, our data from both the two stages of mineralization (stage II and III) are randomly distributed in $^{187}Os/^{188}Os$ vs. $1/^{192}Os$ space (Figs. 11a and b), which means the isochrons we obtain represent the best estimate of the timing of gold mineralization, thus indicating Devonian and Carboniferous gold

mineralization. In addition, samples from the stage Ⅱ vein in the Annage gold deposit yield a Devonian age of 383 ± 8 Ma, which is consistent with the age of the stage Ⅱ vein of the Guoluolongwa gold deposit within uncertainty. The random distribution of the data in $^{187}Os/^{188}Os$ vs. $1/^{192}Os$ space (Fig. 11C) indicate the isochron of the Annage gold deposits should also not be an errorchron or pseudochron (Faure and Mensing, 2005; Yang et al., 2008) and thus the isochron age should represent the formation age of the stage Ⅱ vein of this deposit, which support the Devonian gold mineralizing event occurred in the Gouli area. The Re-Os model date of the sample CK003 (349 ± 6 Ma) from the Annage gold deposit, is identical with the Carboniferous age of stage Ⅲ veins in the Guoluolongwa gold deposit, which further implies that this gold mineralizing event occurred in the Gouli gold field during the Early Carboniferous. Furthermore, the contemporaneous Devonian gold-mineralizing event has been revealed to the north of the East Kunlun Orogen (Qilian-Qaidam; Sericite Ar-Ar, 409-372 Ma; Yang et al., 2005; Zhang et al., 2005), indicating the existence of a Devonian gold-mineralizing event regionally. Consequently, we interpret the two episodes recorded by our Re-Os data from both the Guoluolongwa and Annage gold deposits as the formation ages of stage Ⅱ and Ⅲ veins in the Gouli gold field, respectively. In this context, the early reported muscovite Ar-Ar age is considered to represent a later thermal/hydrothermal activity that may be related to the pervasive Permian-Triassic magmatic event in the East Kunlun Orogen (Chen et al., 2017). Whether this later thermal/hydrothermal activity contribute gold to the two deposits deserve further study. Based on the present evidence, we prefer that the later thermal/hydrothermal activity

(Triassic) is unlikely to contribute significant gold to the two deposits, since a later gold-bearing fluid should affect the Re-Os system of the dating mineral formed early or form new dating mineral (such as gold-bearing pyrite) which is closely relate to gold in the studied area. Our Re-Os data do not record any information of this Triassic event and no new gold-bearing assemblage or vein has been found by field observation.

From a regional perspective, with the exception of the Guoluolongwa and Annage gold deposits that occur in Proterozoic or Ordovician-Silurian metamorphic rocks, the three other gold deposits in the Gouli goldfield crosscut Triassic (Asiha and Delong) or Silurian (Walega) aged intrusions (Fig. 2) and show distinct mineralization styles from those of Guoluolongwa and Annage (Li et al., 2012; Chen, 2018), indicating different gold-mineralizing events forming these deposits. Thus at least one Triassic or post-Triassic gold-mineralizing event occurred in the Gouli goldfield based on the cross-cutting relationship between orebodies and Triassic intrusion (Li et al., 2014), which is likely to be the same Triassic event leading to the formation of the Wulonggou goldfield to the west of the Gouli (Zhang et al., 2017). Consequently, together with the Late Paleozoic (Devonian and Carboniferous) mineralization revealed by our Re-Os data, there are at least two gold-mineralizing epochs (Late Paleozoic and Late Triassic) in the Gouli goldfield.

5.3 Source of ore-forming materials and implications on the genetic model

The geochronological data presented above improve the framework of the temporal relationships between gold mineralization and tectonic-magmatic activities (discussed below) that may directly contribute to the formation of the gold deposits. However, timing constraint

alone does not distinguish between rock types or reservoirs that may have contributed to the formation of these gold deposits. In this regard, the Osi values of the sulfides from the Gouli goldfield can provide a unique insight into the ore-forming process (e.g., Morelli et al., 2007; Morelli et al., 2010).

As discussed above, the non-radiogenic Osi values of the stage Ⅱ (0.12 ± 0.01) and Ⅲ (0.13 ± 0.1) veins in the Guoluolongwa gold deposit are consistent, similar to that of the mantle (Fig. 10; ~0.12–0.13; Shirey and Walker, 1998), indicating mantle or extremely juvenile crustal source of Os, by inference the ore metal (Au). This also excludes the wall rocks of the Naij Tal Group or possibly the concealed Proterozoic metamorphic basement rocks as the sources of the ore-forming materials (Fig. 10). Considering the contemporaneous mantle-derived mafic rocks in the East Kunlun Orogen (345 – 380 Ma; Chen et al., 2001; Bao et al., 2013), we contend that the ore metals of the two vein types of the Guoluolongwa gold deposit were derived from partial melting of the mantle. As to the ore-forming fluids, previously reported H-O isotopes (e.g., Wang, 2012; Yue, 2013; Xiao et al., 2014) indicate they were derived mainly from magmatic sources (Fig. 12) (Chen, 2018). The $\delta^{34}S$ of the Guoluolongwa gold deposit shows a range of -6‰ – 5.2‰ (Chen, 2018 and references therein), a much wider range than that of mantle-derived sulfur ($\delta^{34}S$=0±3‰), indicating crustal sulfur may also contribute to the mineralization. Taker together, the origin of the Guoluolongwa gold deposit is different to that of typical orogenic gold deposits whose ore metal and fluids are considered to be derived from old metamorphic rocks (Goldfarb et al., 2005 and references therein). It is also noteworthy that there is a nominally ~20 Ma age gap

between the formations of the two gold-bearing vein types. Such a large age gap is likely to imply two separately magmatic events contributing to the formation of the two vein types instead of a continuous hydrothermal activity, which could also explain the different mineral assemblages between the two vein types. In summary, the Guoluolongwa gold deposit is considered to be of magmatic origin and formed in relation to multiple magmatic events.

For the Annage gold deposit, considering the close spatial relationship (<3km), contemporaneous mineralization (Figs. 7 – 10), identical mineralization styles and mineral assemblages (Figs. 5 – 6), and consistent H-O isotope compositions (Fig. 12) between the Guoluolongwa and Annage deposits, we contend that the two deposits should have similar origin, which suggests that mantle-derived fluids and metals contributed to the formation of the Annage deposit. However, the Osi values of the sulfides from this deposit are much higher than that of the mantle (~0.12 – 0.13; Shirey and Walker, 1998), indicating another radiogenic source supplied the Os of this deposit. Considering the specific geological background of the two deposits, wall rocks, i.e. the Ordovician-Silurian (Naij Tal Group) and Proterozoic metamorphic rocks (Figs. 3 and 4), are likely candidates leading to the high Osi values of the stage Ⅱ gold-bearing veins. The protoliths of the Ordovician-Silurian metamorphic rocks are mudstone and volcanic rocks that were formed in the marine environment (Chen et al., 2013; Chen et al., 2014). Thus, the mudstone should have a similar initial $^{187}Os/^{188}Os$ ratio with that of the Ordovician-Silurian sea water (0.28-1.08; 449 Ma; Finlay et al., 2010). Considering ~70 Ma (time gap between 449 Ma and 383 Ma) of ^{187}Os ingrowth from ^{187}Re decay, the $^{187}Os/^{188}Os$ ratio of the Ordovician-Silurian black shale (0.6

to 1.9; Fig. 10) is much lower than the Osi value of the stage II veins, indicating that the mudstone is likely not be the sole source of the Os in the stage II veins. Further, the volcanic rocks of the Naij Tal Group that formed at 429 Ma had a similar initial $^{187}Os/^{188}Os$ (429 Ma) ratio with that of the mantle (Feng et al., 2009). Taking into account of the mantle-like initial $^{187}Os/^{188}Os$ ratios and Os accumulation due to ^{187}Re decay, our calculation indicates that the volcanic rocks must have $^{187}Re/^{188}Os > 4600$ to gain high $^{187}Os/^{188}Os$ ratio of 3.65 at 383 Ma, which is unlikely to be true (Shirey and Walker, 1998). Taken together, the Ordovician-Silurian metamorphic rocks (the host rocks of the Guoluolongwa gold deposit) are unlikely to be the main Os source of the stage II vein in the Annage gold deposit, which is consistent with the low initial $^{187}Os/^{188}Os$ ratios of the Guoluolongwa gold deposit. The reported age for the Proterozoic metamorphic rocks in the Gouli area is 904 Ma that represents the age of the protoliths (Fig. 2; Chen et al., 2006). If these rocks are the source of the Os, the Proterozoic metamorphic rocks would have $^{187}Re/^{188}Os$ values between 300 and 500 to produce the observed Osi of the sulfides (Fig. 10). Geological units that have such high $^{187}Re/^{188}Os$ could be basalts or black shales (Shirey and Walker, 1998) that are possible protoliths of the Proterozoic metamorphic rocks given these rocks contain amphibolite and schist (Fig. 4). Thus, it is likely that the Proterozoic metamorphic rocks are the main source of the Os associated with stage II veins, which is supported by that the host rocks of orebody I, where the samples collected, are Proterozoic metamorphic rocks (Fig. 4). Consequently, in addition to the same mineralizing process in the Guoluolongwa gold deposit, the ore-forming fluids of the Annage gold deposit likely reacted with the Proterozoic metamorphic wall rocks that

released leached radiogenic Os to the fluids and changed the initial non-radiogenic Os compositions (0.12 – 0.13) to a radiogenic composition (3.65). However, whether this process added crustal ore metal (Os and Au) to the Annage gold deposit need further study.

5.4 Relationships between gold mineralization and tectonic-magmatic activities and significance on regional exploration

Regionally, two gold-mineralizing epochs are revealed from our Re-Os data (Late Devonian and Early Carboniferous), published Ar-Ar dating and field observations (Triassic; e.g., Zhang et al., 2017). Interestingly, all the gold mineralizing events overlap with emplacement of A-type granites and mafic rocks (Fig. 13), which indicate the extensional regime within the East Kunlun Orogen. Considering the geological background of the East Kunlun Orogen (Chen et al., 2017), the two gold-mineralizing epochs should occur during the post-collisional stages related to the evolution of the Prototethys Ocean and Paleotethys Ocean, respectively (Fig. 13), with the ore-forming fluids being derived from a juvenile magma (Fig. 12). In this context, gold mineralization in the East Kunlun Orogen should be genetically related to post-collisional magmatism that supplied auriferous fluids.

From a more regional perspective, a number of gold deposits have been reported in the adjacent western Qinling (to the immediate west of the East Kunlun Orogen; Figs. 1A and B) (Liu et al., 2015) and Qilian-Qaidam (to the north of the East Kunlun Orogen; Figs. 1 A and B) (Zhang et al., 2005). In these areas, both lode and disseminated gold deposits are present and most of these gold deposits are hosted in Proterozoic – Early Paleozoic (Qilian-Qaidam) (Zhang et al., 2005) and Devonian (western Qinling) (Liu et al., 2015) (metamorphic)

volcanic-sedimentary rocks, similar to those of gold deposits in the East Kunlun Orogen. Many of these gold deposits exhibit similar H-O isotopes with those in the East Kunlun Orogen (Fig. 12), indicating magmatic fluids with minor meteoric water played an important role in the mineralizing process (e.g., Fan et al., 2008; Liu et al., 2015; Zhang et al., 2017). In addition, the currently reported ages of these gold deposits display two peaks (Late Paleozoic and Triassic) of gold mineralization (Fig. 13). These ages, integrated with the geological background, indicate that most of these gold deposits were formed in collisional or post-collisional regime related to the evolution of the Prototethys Ocean and Paleotethys Ocean (Fig. 13). In summary, it is likely that common tectonic-magmatic activities controlled the formation of gold deposits from the East Kunlun Orogen, Qilian-Qaidam and western Qinling, all of which are located in the west of the Central Orogenic Belt (Fig. 1A) that are controlled by the evolution of the Prototethys Ocean and Paleotethys Ocean (Qiu and Wijbrans, 2008; Wu and Zheng, 2013). Thus, considering the common geological background and the gold ore-forming potential of the whole western Central Orogenic Belt, it is possible that more Late Paleozoic gold deposits may be revealed in these areas, especially in the western Qinling where multiple magmatic activities developed, but only indirect dating methods (e.g., Ar-Ar dating of micaceous minerals) have been applied (Fig. 13 and related references).

7. Conclusions

Pyrites and chalcopyrites from gold-bearing ores in the Guoluolongwa gold deposit in the Gouli goldfield yield Re-Os ages of 375 ± 11 Ma for the stage II pyrite-quartz vein and 354 ±

7 Ma for the stage III polymetallic sulfides-quartz vein, which are also recorded by the stage II pyrites from the adjacent Annage gold deposit (383 ± 6 Ma and 349 ± 6 Ma). These data, together with field observations indicate that at least three gold mineralizing events (two in Late Paleozoic and one in Late Triassic) occurred in the Gouli goldfield. The Osi values of sulfides indicate that Os and by inference, the ore metal (Au) of the Guoluolongwa deposits were derived from mantle-derived magma. A common ore metal source is also recommended for the Annage gold deposit, but the Os of this deposit is considered to be derived from both the mantle and Proterozoic wall rocks. Results from this study together with previously reported ages of gold mineralization in the East Kunlun Orogen and adjacent areas, indicate that there are two gold-mineralizing epochs (Late Paleozoic and Late Triassic) in the west of the Central Orogenic Belt (included western Qinling, East Kunlun Orogen and Qaidam-Qilian) and all gold mineralizing events occurred in collisional or post-collisional setting related to Tethyan evolution that controlled the whole Central Orogenic Belt. Thus, we infer that more Late Paleozoic gold deposits may be present in the west of Central Orogenic Belt.

8. Acknowledgments

This research was jointly supported by the Fundamental Research Funds for the Central Universities (CUGL17043), the Funds from the East China University of Technology (DHBK2018009 and GJJ180387), and the China Geological Survey (12120114081401, 12120114000701). DS acknowledges the Total Endowment Fund. We appreciate fieldwork assistance of Shaoqing Zhao, Zhen Wang, Xiaolong Wang, Yang Tang, Junlin Chen, Yujing Zhao, and Yan Liu from the China University of Geosciences.

References

Bao, G.P., Wang, G.L., Liu, R., Han, H.C., 2013, Kayakedengtage area two basic dike rocks geochemistry and significance: Northwestern Geology, v. 46, p. 37-43 (in Chinese with English abs.).

Bian, Q.T., Li, D.H., Pospelov, I., Yin, L.M., Li, H.S., Zhao, D.S., Chang, C.F., Luo, X.Q., Gao, S.L., Astrakhantsev, O., Chamov, N., 2004, Age, geochemistry and tectonic setting of Buqingshan ophiolites, North Qinghai-Tibet Plateau, China: Journal of Asian Earth Sciences, v. 23, p. 577-596.

Chen, J., Wei, J., Fu, L., Li, H., Zhou, H., Zhao, X., Zhan, X., Tan, J., 2017, Multiple sources of the Early Mesozoic Gouli batholith, Eastern Kunlun Orogenic Belt, northern Tibetan Plateau: Linking continental crustal growth with oceanic subduction: Lithos, v. 292-293, p. 161-178.

Chen, L., Sun, Y., Pei, X.Z., Gao, M., Tao, F., Zhang, Z.Q., Chen, W., 2001, Northernmost Paleo-Tethyan oceanic basin in Tibet: geochronological evidence from 40Ar/39Ar age dating of Dur'ngoi ophiolite: Chinese Science Bulletin, v. 46, p. 1203-1205.

Chen, X.H., Gehrels, G., An, Y., Li, L., Jiang, R.B., 2012, Paleozoic and Mesozoic basement magmatisms of Eastern Qaidam Basin, Northern Qinghai-Tibet Plateau: LA-ICP-MS zircon U-Pb geochronology and its geological significance: Acta Geologica Sinica, v. 86, p. 350-369.

Chen, G.J., 2014, Metallogenesis of gold deposits in Gouli regional and peripheral area of East Kunlun, Qinghai province: Ph.D. thesis, Changchun, Jilin University, 165p (in

Chinese with English abs.).

Chen, J., 2018, Paleozoic-Mesozoic tectono-magmatic evolution and gold mineralization in Gouli Area, east end of East Kunlun Orogen: Ph.D. thesis, Wuhan, China University of Geosciences, 224p (in Chinese with English abs.).

Chen, J.J., Fu, L.B., Wei, J.H., Tian, N., Xiong, L., Zhao, Y.J., Zhang, Y.J., Qi, Y.Q., 2016, Geochemical characteristics of Late Ordovician granodiorite in Gouli area, Eastern Kunlun Orogenic Belt, Qinghai province: Implications on the evolution of Proto-Tethys Ocean: Earth Science, v. 41, p. 1863-1882 (in Chinese with English abs.).

Chen, N.S., Li, X.Y., Wang, X.Y., Chen, Q., Wang, Q.Y., Wan, Y.S., 2006, Zircon SHRIMP U-Pb age of Neoproterozoic metagranite in the North Kunlun unit on the southern margin of the Qaidam block in China: Geological Bulletin of China, v. 25, p. 1311-1314 (in Chinese with English abs.).

Chen, Y.X., Pei, X.Z., Li, R.B., Li, Z.C., Pei, L., Chen, G.C., Liu, C.J., Li, X.B., Yang, J., 2013, Zircon U-Pb age, geochemical characteristics and tectonic significance of metavolcanic rocks from Naij Tal Group, east section of East Kunlun: Earth Science Frontier, v. 20, p. 240-254 (in Chinese with English abs.).

Chen, Y.X., Pei, X.Z., Li, R.B., Li, Z.C., Pei, L., Liu, C.J., Yang, J., 2014, Geochemical characteristics and tectonic significance of meta-sedimentary rocks from Naij Tal group，eastern section of East Kunlun: Geoscience, v. 28, p. 489-500 (in Chinese with English abs.).

Cumming, V.M., Poulton, S.W., Rooney, A.D., Selby, D., 2013, Anoxia in the terrestrial

environment during the late Mesoproterozoic: Geology, v. 41, p. 583-586.

Ding, C.M., 2007, Genesis of Tanjianshan gold deposit: Qinghai Science and Technology, p. 32-36 (in Chinese with English abs.).

Ding, Q.F., Jin, S.K., Wang, G., Zhang, B.L., 2013, Ore-Forming fluid of the Guoluolongwa gold deposit in Dulan county, Qinghai province: Journal of Jilin University (Earth Science Edition), v. 43, p. 415-426 (in Chinese with English abs.).

Esser, B.K., Turekian, K.K., 1993, The osmium isotopic composition of the continental crust: Geochimica Et Cosmochimica Acta, v. 57, p. 3093-3104.

Fan, J.J., Lu, Y.M., Cong, Y.X., Chang, C.J., 2008, Study on 3 gold deposits varied in characteristics at the north slope of the Danghe Nanshan Mountain in the west Qilian Mountains: Contributions To Geology and Mineral Resources Research, v. 23, p. 48-53 (in Chinese with English abs.).

Fan, J.J., Zhang, X.J., Chang, C.J., Zhang, H.Y., Cong, Y.X., Ren, S., 2006, Geochemistry and genesis of the Jijiaogou gold deposit in Subei, Gansu Province, China: Geology and Resources, v. 15, p. 272-276 (in Chinese with English abs.).

Faure, G., Mensing, T.M., 2005, Isotopes: principles and applications: 3 ed. Hoboken, New Jersey, John Wiley & Sons, 897p.

Feng, C.Y., Qu, W.J., Zhang, D.Q., Dang, X.Y., Du, A.D., Li, D.X., She, H.Q., 2009, Re–Os dating of pyrite from the Tuolugou stratabound Co(Au) deposit, eastern Kunlun Orogenic Belt, northwestern China: Ore Geology Reviews, v. 36, p. 213-220.

Feng, C.Y., 2002, Multiple orogenic processes and mineralization of orogenic gold deposits

in the East Kunlun Orogen, Qinghai province: Ph.D. thesis, Beijing, Chinese Academy of Geological Sciences, 104p (in Chinese with English abs.).

Feng, C.Y., Zhang, D.Q., Wang, F.C., Li, D.X., She, H.Q., 2004, Geochemical characteristics of ore-forming fluids from the orogenic An (and Sb) deposits in the eastern Kunlun area, Qinghai province: Acta Petrologica Sinica, v. 20, p. 949-960 (in Chinese with English abs.).

Feng, J.Y., Pei, X.Z., Yu, S.L., Ding, S.P., Li, R.B., Sun, Y., Zhang, Y.F., Li, Z.C., Chen, Y.X., Zhang, X.F., Chen, G.C., 2010, The discovery of the mafic-ultramafic melange in Kekesha area of Dulan County, East Kunlun region, and its LA-ICP-MS zircon U-Pb age: Geology in China, v. 37, p. 28-38 (in Chinese with English abs.).

Finlay, A.J., Selby, D., Gr Cke, D.R., 2010, Tracking the Hirnantian glaciation using Os isotopes: Earth and Planetary Science Letters, v. 293, p. 339-348.

Goldfarb, R.J., Baker, T., Dube, B., Groves, D.I., Hart, C.J., Gosselin, P., 2005, Distribution, character, and genesis of gold deposits in metamorphic terranes: Economic Geology 100th Anniversary Volume, p. 407-450.

He, D.F., Dong, Y.P., Zhang, F.F., Yang, Z., Sun, S.S., Cheng, B., Zhou, B., Liu, X.M., 2016, The 1.0 Ga S‐type granite in the East Kunlun Orogen, Northern Tibetan Plateau: Implications for the Meso‐to Neoproterozoic tectonic evolution: Journal of Asian Earth Sciences, v. 130, p. 46-59.

Hu, R.G., 2008, Research on geological-Geochemical characteristics and Genesis of the Guoluolongwa gold deposit in Qinghai Province: master thesis, Changsha, Central South

University, 99p (in Chinese with English abs.).

Kong, H.L., Li, J.C., Li, Y.Z., Jia, Q.Z., Yang, B.R., 2014, Geochemistry and zircon U-Pb geochronology of Annage diorite in the eastern section from East Kunlun in Qinghai province: Geological Science and Technology Information, v. 33, p. 11-17 (in Chinese with English abs.).

Lawley, C., Selby, D., Imber, J., 2013, Re-Os molybdenite, pyrite, and chalcopyrite geochronology, Lupa goldfield, southwestern Tanzania: tracing metallogenic time scales at midcrustal shear zones hosting orogenic Au deposits: Economic Geology, v. 108, p. 1591-1613.

Li, R.B., Pei, X.Z., Li, Z.C., Pei, L., Liu, C.J., Chen, Y.X., Chen, G.C., Liu, Z.Q., Yang, J., 2015, Geochemistry and zircon U–Pb geochronology of granitic rocks in the Buqingshan tectonic mélange belt, northern Tibet Plateau, China and its implications for Prototethyan evolution: Journal of Asian Earth Sciences, v. 105, p. 374-389.

Li, R.B., Pei, X.Z., Li, Z.C., Sun, Y., Feng, J.Y., Lei, P., Chen, G.C., Liu, C.J., Chen, Y.X., 2013, Geochemical features, age, and tectonic significance of the Kekekete mafic-ultramafic rocks, East Kunlun Orogen, China: Acta Geologica Sinica, v. 87, p. 1319-1333.

Li, B.Y., Shen, X., Chen, G.J., Yang, Y.Q., Li, Y.S., 2012, Geochemical features of ore-forming fluids and metallogenesis of vein Ⅰ in Asiha gold ore deposit, Eastern Kunlun, Qinghai province: Journal of Jilin University (Earth Science Edition), v. 42, p. 1676-1687 (in Chinese with English abs.).

Li, B.Y., Sun, F.Y., Yu, X.F., Qian, Y., Wang, G., Yang, Y.Q., 2012, U-Pb dating and geochemistry of diorite in the eastern section from eastern Kunlun middle uplifted basement and granitic belt: Acta Petrologica Sinica, v. 28, p. 1163-1172 (in Chinese with English abs.).

Li, H.M., Wang, C.L., Liu, Z.W., Liu, J.Q., 2003, Two different kinds of gold deposits on northern slope of Danghenanshan area in South Qilian Mountains: Mineral Deposits, v. 22, p. 191-198 (in Chinese with English abs.).

Li, J.C., Jia, Q.Z., Du, W., Su, Y.Z., Kong, H.L., Nan, K.E.W., Yang, B.R., 2014, LA-ICP-MS zircon dating and geochemical characteristics of quartz diorite in Asiha gold deposit in east segment of the Eastern Kunlun: Journal of Jilin University (Earth Science Edition), v. 44, p. 1188-1199 (in Chinese with English abs.).

Li, W.Y., 2008, Geochronology and geochemistry of the ophiolites and island-arc-type igneous rocks in the Western Qinling orogen and the Eastern Kunlun orogen: implication for the evolution of the Tethyan Ocean: Ph.D. thesis, Hefei, University of Science and Technology of China, 1-174p (in Chinese with English abs.).

Liu, J., Liu, C., Carranza, E.J.M., Li, Y., Mao, Z., Wang, J., Wang, Y., Zhang, J., Zhai, D., Zhang, H., Shan, L., Zhu, L., Lu, R., 2015, Geological characteristics and ore-forming process of the gold deposits in the western Qinling region, China: Journal of Asian Earth Sciences, v. 103, p. 40-69.

Liu, L., Liao, X.Y., Wang, Y.W., Wang, C., Santosh, M., Yang, M., Zhang, C.L., Chen, D.L., 2016, Early Paleozoic tectonic evolution of the North Qinling Orogenic Belt in Central

China: Insights on continental deep subduction and multiphase exhumation: Earth-Science Reviews, v. 159, p. 58-81.

Liu, C.D., Zhang, W.Q., Mo, X.X., Luo, Z.H., Yu, X.H., Li, S.W., Zhao, X., 2002, Features and origin of mafic microgranular enclaves in the Yuegelu granite in the Eastern Kunlun: Geological Bulletin of China, v. 21, p. 739-744 (in Chinese with English abs.).

Liu, S., Li, J., Li, Y., Li, D., Zhang, A., He, S., 2016, Geochemical Characteristics of the Volcanic Rocks from the Maoniushan Formation in the Dadakenwulashan Pb-Zn Deposit, East Kunlun and Its Significance: Northwestern Geology, v. 49, p. 11-24 (in Chinese with English abs.).

Liu, Z.Q., Pei, X.Z., Li, R.B., Li, Z.C., Zhang, X.F., Liu, Z.G., Chen, G.C., Chen, Y.X., Ding, S.P., Guo, J.F., 2011, LA-ICP-MS zircon U-Pb geochronology of the two suites of ophiolites at the Buqingshan area of the A'nyemaqen Orogenic Belt in the southern margin of East Kunlun and its tectonic implication: Acta Geologica Sinica, v. 85, p. 185-194 (in Chinese with English abs.).

Lu, L., Wu, Z.H., Hu, D.G., Patrick, J.B., Hao, S., Zhou, C.J., 2010, Zircon U-Pb age for rhyolite of the Maoniushan Formation and its tectonic significance in the East Kunlun Mountains: Acta Petrologica Sinica, v. 26, p. 1150-1158 (in Chinese with English abs.).

Lu, L., Zhang, Y.L., Wu, Z.H., Hu, D.G., 2013, Zircon U-Pb dating of Early Paleozoic granites from the East Kunlun Mountains and its geological significance: Acta Geoscientica Sinica, v. 34, p. 447-454 (in Chinese with English abs.).

Ludwig, K.R., 2012, User's manual for Isoplot 3.75——A geochronological toolkit for

Microsoft Excel: Berkeley, Berkeley Geochronology Center Special Publication No. 5, 1-75p.

Ma, C.Q., Xiong, F.H., Yin, S., Wang, L.X., Gao, K., 2015, Intensity and cyclicity of orogenic magmatism: An example from a Paleo-Tethyan granitoid batholith， Eastern Kunlun，northern Qinghai-Tibetan Plateau: Acta Petrologica Sinica, v. 31, p. 3555-3568 (in Chinese with English abs.).

Mao, J.W., Zhang, Z.H., Yang, J.M., Wang, Z.L., 2000, Fluid inclusions of shear zone type gold deposits in the western part of North Qilian Mountain: Mineral Deposits, v. 19, p. 9-16 (in Chinese with English abs.).

Meisel, T., Walker, R.J., Morgan, J.W., 1996, The osmium isotopic composition of the Earth's primitive upper mantle: Nature, v. 383, p. 517-520.

Meng, F.C., Cui, M.H., Wu, X.K., Wu, J.F., Wang, J.H., 2013, Magmatic and metamorphic events recorded in granitic gneisses from the Qimantag， East Kunlun Mountains，Northwest China: Acta Petrologica Sinica, v. 29, p. 2107-2122 (in Chinese with English abs.).

Mo, X.X., Luo, Z.H., Deng, J.F., Yu, X.H., Liu, C.D., Chen, H.W., Yuan, W.M., Liu, Y.H., 2007, Granitoids and crustal growth in the East-Kunlun Orogenic Belt: Geological Journal of China Universities, v. 13, p. 403-414 (in Chinese with English abs.).

Morelli, R., Creaser, R.A., Seltmann, R., Stuart, F.M., Selby, D., Graupner, T., 2007, Age and source constraints for the giant Muruntau gold deposit, Uzbekistan, from coupled Re-Os-He isotopes in arsenopyrite: Geol, v. 35, p. 795.

Morelli, R.M., Bell, C.C., Creaser, R.A., Simonetti, A., 2010, Constraints on the genesis of gold mineralization at the Homestake Gold Deposit, Black Hills, South Dakota from rhenium–osmium sulfide geochronology: Mineralium Deposita, v. 45, p. 461-480.

Morelli, R.M., Creaser, R.A., Bell, C.C., 2005, Re-Os arsenopyrite geochronology of the Homestake gold deposit, Black Hills, South Dakota, and implication for chronometer closure temperature: Salt Lake City.

Nowell, G.M., Luguet, A., Pearson, D.G., Horstwood, M.S.A., 2008, Precise and accurate 186 Os/ 188 Os and 187 Os/ 188 Os measurements by multi-collector plasma ionisation mass spectrometry (MC-ICP-MS) part I: Solution analyses: Chemical Geology, v. 248, p. 363-393.

Qi, X.P., Yang, J., Fan, X.G., Cui, J.T., Cai, Z.F., Zeng, X.W., Wei, W., Qu, X.X., Zai, L.M., 2016, Age, geochemical characteristics and tectonic significance of Changshishan ophiolite in central East Kunlun tectonic mélange belt along the east section of East Kunlun Mountains: Geology in China, v. 43, p. 797-816 (in Chinese with English abs.).

Qiu, H.N., Wijbrans, J.R., 2008, The Paleozoic metamorphic history of the Central Orogenic Belt of China from 40 Ar/39 Ar geochronology of eclogite garnet fluid inclusions: Earth and Planetary Science Letters, v. 268, p. 501-514.

Selby, D., 2007, Direct Rhenium-Osmium age of the Oxfordian-Kimmeridgian boundary, Staffin bay, Isle of Skye, U.K., and the Late Jurassic time scale: Norwegian Journal of Geology, v. 29, p. 291-299.

Selby, D., Creaser, R.A., 2004, Macroscale NTIMS and microscale LA-MC-ICP-MS Re-Os

isotopic analysis of molybdenite: Testing spatial restrictions for reliable Re-Os age determinations, and implications for the decoupling of Re and Os within molybdenite: Geochimica Et Cosmochimica Acta, v. 68, p. 3897-3908.

Selby, D., Creaser, R.A., Hart, C., Rombach, C.S., Thompson, J., Smith, M.T., Bakke, A.A., Goldfarb, R.J., 2002, Absolute timing of sulfide and gold mineralization: A comparison of Re-Os molybdenite and Ar-Ar mica methods from the Tintina Gold Belt, Alaska: Geology, v. 30, p. 791-794.

Selby, D., Kelley, K.D., Hitzman, M.W., Zieg, J., 2009, Re–Os sulfide (bornite, chalcopyrite, and pyrite) systematics of the carbonate-hosted copper deposits at Ruby Creek, southern Brooks range, Alaska: Economic Geology, v. 104, p. 437-444.

Shirey, S.B., Walker, R.J., 1998, The Re-Os isotope system in cosmochemistry and high-temperature geochemistry: Annual Review of Earth and Planetary Sciences, v. 26, p. 423-500.

Song, S., Niu, Y., Su, L., Zhang, C., Zhang, L., 2014, Continental orogenesis from ocean subduction, continent collision/subduction, to orogen collapse, and orogen recycling: The example of the North Qaidam UHPM belt, NW China: Earth-Science Reviews, v. 129, p. 59-84.

Stein, H., Scherstén, A., Hannah, J., Markey, R., 2003, Subgrain-scale decoupling of Re and 187 Os and assessment of laser ablation ICP-MS spot dating in molybdenite: Geochimica Et Cosmochimica Acta, v. 67, p. 3673-3686.

Stein, H.J., Morgan, J.W., Scherstén, A., 2000, Re-Os dating of low-level highly radiogenic

(LLHR) sulfides: The Harnas gold deposit, southwest Sweden, records continental-scale tectonic events: Economic Geology, v. 95, p. 1657-1671.

Tao, J.J., 2014, Characteristics of fluid inclusions and genesis of Annage gold deposit, Qinghai Province: master thesis, Changsha, Central South University, 66p (in Chinese with English abs.).

Wang, G.C., Chen, N.S., Zhu, Y.H., Zhang, K.X., 2003, Late Caledonian ductile thrusting deformation in the Central East Kunlun Belt, Qinghai, China and its significance: evidence from geochronology: Acta Geologica Sinica, v. 77, p. 311-319.

Wang, J., Li, J., Zhao, X., Ma, C., Qu, W., Du, A., 2008, Re-Os dating of pyrrhotite from the Chaoshan gold skarn, eastern Yangtze craton, eastern China: International Geology Review, v. 50, p. 392-406.

Wang, G., 2012, Study on geological characteristics and genesis of Guoluolongwa gold deposit in Qinghai province: master thesis, Changchun, Jilin University, 86p (in Chinese with English abs.).

Wei, B., 2015, Study on the geological characteristic and tectonic attribute of the ophiolite and island-arc-type igneous rocks, central belt of East Kunlun (eastern section): master thesis, Xi'an, Chang'an University, 141p (in Chinese with English abs.).

Wei, X.L., Zhang, D.X., Gan, C.P., Chen, L.B., 2016, Discovery and geological significance of Neoproterozoic intrusive body in the Kaerqueka area of the East Kunlun mountain: Contributions to Geology and Mineral Resources Research, v. 31, p. 236-244 (in Chinese with English abs.).

Wu, Y.B., Zheng, Y.F., 2013, Tectonic evolution of a composite collision orogen: An overview on the Qinling–Tongbai–Hong'an–Dabie–Sulu orogenic belt in central China: Gondwana Research, v. 23, p. 1402-1428.

Xia, R., Wang, C., Qing, M., Deng, J., Carranza, E.J.M., Li, W., Guo, X., Ge, L., Yu, W., 2015, Molybdenite Re-Os, zircon U-Pb dating and Hf isotopic analysis of the Shuangqing Fe-Pb-Zn-Cu skarn deposit, East Kunlun Mountains, Qinghai Province, China: Ore Geology Reviews, v. 66, p. 114-131.

Xia, R., Wang, C.M., Qing, M., Li, W.L., Carranza, E.J.M., Guo, X.D., Ge, L.S., Zeng, G.Z., 2015, Zircon U-Pb dating, geochemistry and Sr-Nd-Pb-Hf-O isotopes for the Nan'getan granodiorites and mafic microgranular enclaves in the East Kunlun Orogen: record of closure of the Paleo-Tethys: Lithos, v. 234, p. 47-60.

Xiao, Y., Feng, C.Y., Li, D.X., Liu, J.N., 2014, Chronology and fluid inclusions of the Guoluolongwa gold deposit in Qinghai province: Acta Geologica Sinica, v. 88, p. 895-902 (in Chinese with English abs.).

Yang, J.S., Robinson, P.T., Jiang, C.F., Xu, Z.Q., 1996, Ophiolites of the Kunlun Mountains, China and their tectonic implications: Tectonophysics, v. 258, p. 215-231.

Yang, S.H., Qu, W.J., Tian, Y.L., Chen, J.F., Yang, G., Du, A.D., 2008, Origin of the inconsistent apparent Re–Os ages of the Jinchuan Ni–Cu sulfide ore deposit, China: Post-segregation diffusion of Os: Chemical Geology, v. 247, p. 401-418.

Yang, J.G., Yang, L.H., Ren, Y.X., Li, Z.P., Song, Z.B., 2005, Isotopic Geochronology of the ore-forming process in the Hanshan gold deposit of the North Qilian Mountains: Acta

Geoscientica Sinica, v. 26, p. 315-320 (in Chinese with English abs.).

Yang, X.B., Yang, B.R., Wang, X.Y., 2006, Gold occurrence in Guoluolongwa gold deposit of Qinghai Province: Geology and Prospecting, v. 42, p. 57-59 (in Chinese with English abs.).

Ying, H.F., Zhang, K.X., 2003, Regional geological survey report of People's Republic of China: Dongjicuonahu (I47C001002, Scale: 1:250000): Wuhan, China University of Geosciences Press, 457p (in Chinese).

Yue, W.H., 2013, Geological, geochemical and genetic study of typical deposits from Gouli gold field, Eastern of East Kunlun: Ph.D. thesis, Kunming, Kunming University of Science and Technology, 207p (in Chinese with English abs.).

Yue, W.H., Gao, J.G., Zhou, J.X., 2013, LA-ICP-MS Zircon U-Pb Ages and Lithogeochemistry of Basic Dykes in the Guoluolongwa gold ore Field, Qinghai Province, China: Journal of Mineralogy and Petrology, v. 33, p. 93-102 (in Chinese with English abs.).

Yue, W.H., Zhou, J.X., Gao, J.G., Huang, Y.H., Jia, F.J., 2017, Geochemistry，zircon U-Pb chronology and geological implications of Sederi diabase，Dulan county，Qinghai province: Bulletin of Mineralogy，Petrology and Geochemistry, v. 36, p. 270-278 (in Chinese with English abs.).

Zhang, J., Ma, C., Li, J., Pan, Y., 2017, A possible genetic relationship between orogenic gold mineralization and post-collisional magmatism in the eastern Kunlun Orogen, western China: Ore Geology Reviews, v. 81, p. 342-357.

Zhang, J.Y., Ma, C.Q., Xiong, F.H., Liu, B., Li, J.W., Pan, Y.M., 2014, Early Paleozoic high-Mg diorite-granodiorite in the eastern Kunlun Orogen, western China: Response to continental collision and slab break-off: Lithos, v. 210-211, p. 129-146.

Zhou, Z., Mao, S., Chen, Y., Santosh, M., 2016, U–Pb ages and Lu–Hf isotopes of detrital zircons from the southern Qinling Orogen: Implications for Precambrian to Phanerozoic tectonics in central China: Gondwana Research, v. 35, p. 323-337.

Zhang, D.Q., Dang, X.Y., She, H.Q., Li, D.X., Feng, C.Y., Li, J.W., 2005, Ar-Ar dating of orogenic gold deposits in northern margin of Qaidam and East Kunlun Mountains and its geological significance: Mineral Deposits, v. 24, p. 87-98 (in Chinese with English abs.).

Zhang, D.Q., Feng, C.Y., Li, D.X., Xu, W.Y., Yan, S.H., She, H.Q., Dong, Y.J., Cui, Y.H., 2001, Orogenic gold deposits in the north Qaidam and East Kunlun Orogen, west China: Mineral Deposits, v. 20, p. 137-146 (in Chinese with English abs.).

Zhang, Y.L., Hu, D.G., Shi, Y.R., Lu, L., 2010, SHRIMP zircon U-Pb ages and tectonic significance of Maoniushan Formation volcanic rocks in East Kunlun orogenic belt, China: Geological Bulletin of China, v. 29, p. 1614-1618 (in Chinese with English abs.).

Zhao, C.S., 2004, Gold, silver metallogeny in Eastern Kunlun Orogenic Belt, Qinghai province: Ph.D. thesis, Changchun, Jilin University, 144p (in Chinese with English abs.).

Zhao, J.W., 2008, Study on orogenic gold metallogenic series in Eastern Kunlun Orogenic Belt, Qinghai Province: Ph.D. thesis, Changchun, Jilin University, 189p (in Chinese with English abs.).

Zhu, Y.H., Pan, Y.M., Zhang, K.X., Chen, N.S., Wang, G.C., Hou, G.J., 2000, Mineralogical

characteristics and petrogenesis of ophiolites in East Kunlun Orogenic Belt, Qinghai Province: Acta Mineralogica Sinica, v. 20, p. 128-142 (in Chinese with English abs.).

Figure captions

Fig. 1 (A) Tectonic map of China showing the location of Central Orogenic Belt and significant gold producing areas (after Li et al., 2015). (B) Tectonic divisions of the Qinghai-Tibetan plateau showing the location of the East Kunlun Orogen (after Xia et al., 2015). (C) Simply Geological map of the East Kunlun Orogen showing the main gold deposits/fields (after Xia et al., 2015).

Fig. 2 Geological map of the Gouli goldfield showing the distribution of the main gold deposits (after unpublished geological report). Ages labeled on the map are zircon U-Pb ages and the related references are as follows: (1) (Chen et al., 2012); (2) (Liu et al., 2002); (3) (J.J. Chen et al. in prep.); (4) (Ying and Zhang, 2003); (5) (our unpublished data); (6) (Chen et al., 2016); (7) (our unpublished data); (8) (Li et al., 2012); (9) (Yue et al., 2017); (10) (Chen et al., 2006).

Fig. 3 (A) Geological map of the Guoluolongwa gold deposit showing the locations of the main gold orebodies and the profile A-B. (B) Representative cross-section in the Guoluolongwa gold deposit (after unpublished geological report). Ages in (A) are zircon U-Pb ages from our unpublished data and Yue et al. (2013).

Fig. 4 (A) Geological map of the Annage gold deposit showing the distribution of the main gold orebodies and the location of profile A-B (after Chen, 2014). (B) Representative cross-

section in the Annage gold deposit (after unpublished geological report). Age of diorite in (A) is zircon U-Pb age from Kong et al. (2014).

Fig. 5 Photographs and photomicrographs showing representative veins and minerals in the Guoluolongwa (A-I) and Annage (J-L) gold deposits. (A) Crosscutting relationship of the pyrite-quartz vein, polymetallic sulfides-quartz vein, gabbro, and phyllite. (B) Pyrite-quartz vein cutting cross early quartz vein. (C) Polymetallic sulfides-quartz ore. (D) Native gold-chalcopyrite-sphalerite vein filling the crack of pyrite. (E) Native gold occurring between sphalerite and quartz grains. (F) Chalcopyrite-galena vein; (G) Eutectoid of sphalerite and chalcopyrite. (H) Polymetallic sulfides-quartz vein cut cross early pyrite-quartz vein. (I) Polymetallic sulfides-quartz vein. (J) Pyrite-quartz vein with local massive pyrite. (K) Pyrite-quartz ore. (L) Coarse pyrite.

Fig. 6 Mineral paragenetic sequence of Guoluolongwa and Annage deposits.

Fig. 7 Re-Os plots of stage II pyrite-quartz vein in the Guoluolongwa gold deposit: (A) $^{187}Re/^{188}Os$ vs. $^{187}Os/^{188}Os$ plot; (B) ^{187}Re vs. $^{187}Os^{r}$ plot; (C) Weight average of Re-Os model dates.

Fig. 8 Re-Os plots of stage Ⅲ polymetallic sulfides-quartz vein in the Guoluolongwa gold deposit: (A) $^{187}Re/^{188}Os$ vs. $^{187}Os/^{188}Os$ plot; (B) ^{187}Re vs. $^{187}Os^{r}$ plot; (C) Weight average of Re-Os model dates.

Fig. 9 Re-Os plots of stage gold-bearing vein in the Annage gold deposit: (A) $^{187}Re/^{188}Os$ vs. $^{187}Os/^{188}Os$ plot; (B) ^{187}Re vs. $^{187}Os^{r}$ plot; (C) Weight average of Re-Os model dates.

Fig. 10 Initial $^{187}Os/^{188}Os$ vs. T (Ma) of sulfides from the Guoluolongwa (A, B) and Annage (C) gold deposits. The number "48" overriding the grey lines is the present-day continental crustal $^{187}Re/^{188}Os$ value used for calculating evolution lines of crust with different ages (Esser and Turekian, 1993). The numbers 300 and 500 overriding orange lines are assumed present-day $^{187}Re/^{188}Os$ values used for calculating corresponding crustal evolution lines. Present-day $^{187}Os/^{188}Os$ and $^{187}Re/^{188}Os$ values used for calculating the primitive upper mantle evolution line are 0.1290 and 0.428, respectively (Meisel et al., 1996). Os composition of the Ordovician black shales is also shown for comparison (Finlay et al., 2010). The initial $^{187}Os/^{188}Os$ ratios present here are from samples with $\%^{187}Os^{r} < 90\ \%$.

Fig. 11 initial $^{187}Os/^{188}Os$ vs. 1/Os of sulfides from Guoluolongwa (A, B) and Annage (C) gold deposits. The initial $^{187}Os/^{187}Os$ ratios used were calculated back to 202.7 Ma (Xiao et al., 2014).

Fig. 12 H-O isotopic characteristics of Guoluolongwa and Annage gold deposits. The H-O isotopic data of the Guoluolongwa and Annage gold deposit are from Yue (2013), Xiao et al. (2014), Wang (2012), Hu (2008) and Tao (2014). H-O isotopic data of gold deposits from the East Kunlun Orogen (Feng et al., 2004; Zhao, 2008; Li et al., 2012; Tao, 2014), western Qinling (Liu et al., 2015 and references therein) and Qaidam-Qilian (Mao et al., 2000; Li et al., 2003; Fan et al., 2006; Ding, 2007) are also shown for comparison. GLLW- Guoluolongwa gold deposit; ANG- Annage gold deposit; EKO- East Kunlun Orogen.

Fig. 13 Temporal distribution of gold deposits from East Kunlun Orogen, western Qinling and Qaidam-Qilian. A-type granites and related mafic rocks from East Kunlun Orogen are also shown indicating post-collisional extensional setting for gold deposits. The period of collision/post-collision of the East Kunlun Orogen (Chen et al., 2017 Chen et al., in preparation), western Qinling (Liu et al., 2016; Zhou et al., 2016) and Qaidam-Qilian (Song et al., 2014) are also marked. The sources of ages of gold deposits, A-type granites, and related mafic rocks are summarized in the appendix.

Fig. 1

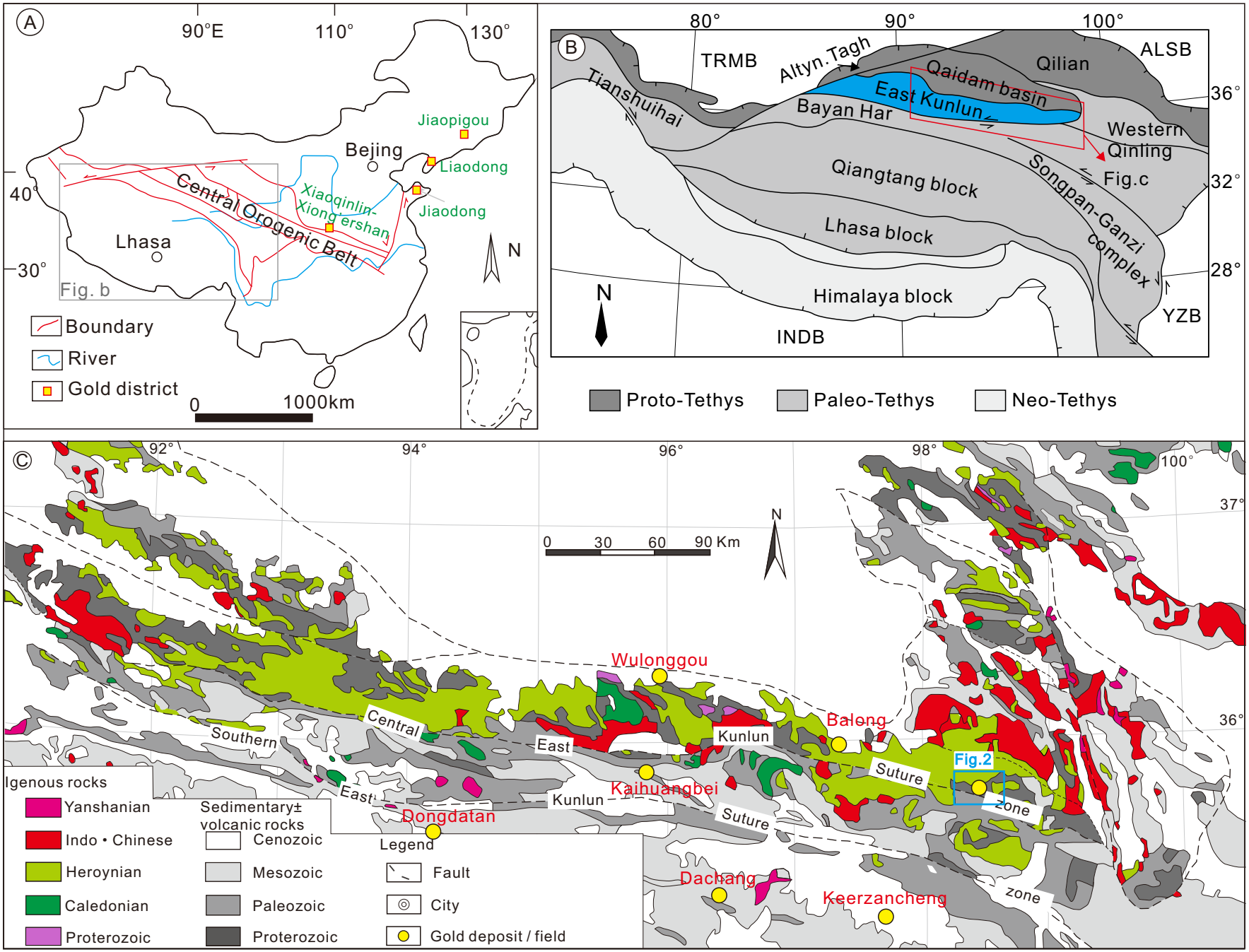
A
90°E
110°
130°
40°
30°
Jiaopigou
Bejing
Liaodong
Jiaodong
Xiaoqinlin-
Xiong'ershan
Central Orogenic Belt
Lhasa
Fig. b
N
Boundary
River
Gold district
0
1000km
B
80°
90°
100°
TRMB
Altyn.Tagh
Qilian
ALSB
Tianshuihai
Qaidam basin
East Kunlun
Bayan Har
Western
Qinling
36°
Fig.c
Qiangtang block
Songpan-Ganzi
complex
32°
Lhasa block
28°
N
Himalaya block
YZB
INDB
Proto-Tethys
Paleo-Tethys
Neo-Tethys
C
92°
94°
96°
98°
100°
37°
36°
N
0
30
60
90 Km
Wulonggou
Balong
Central
Southern
East
Kunlun
Fig.2
Suture
zone
Kaihuangbei
East
Kunlun
Suture
zone
Dongdatan
Dachang
Keerzancheng
Igenous rocks
Yanshanian
Indo • Chinese
Heroynian
Caledonian
Proterozoic
Sedimentary± volcanic rocks
Cenozoic
Mesozoic
Paleozoic
Proterozoic
Legend
Fault
City
Gold deposit / field

Fig. 2

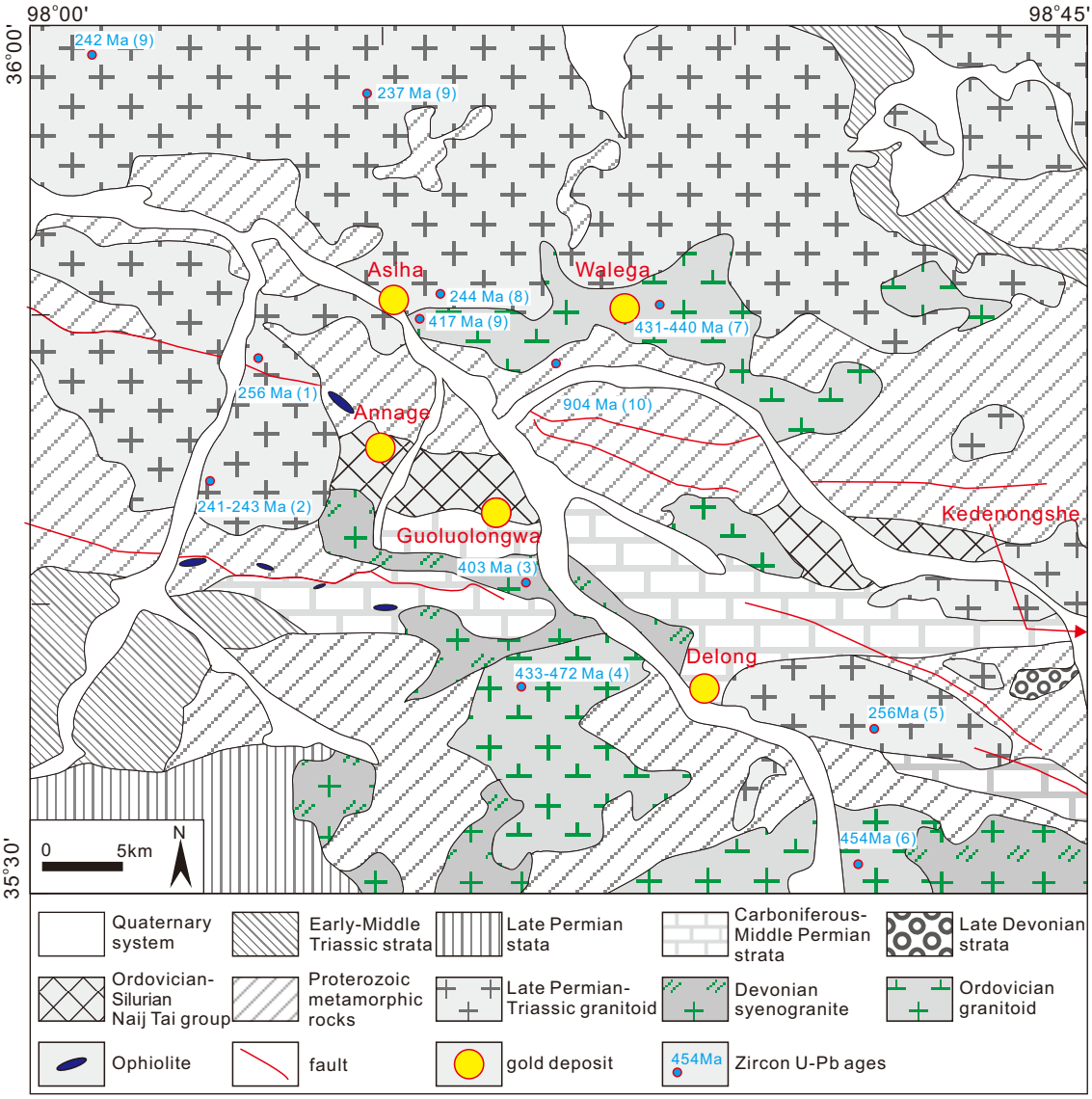
98°00'
98°45'
36°00'
35°30'
242 Ma (9)
237 Ma (9)
Aslha
Walega
244 Ma (8)
417 Ma (9)
431-440 Ma (7)
256 Ma (1)
Annage
904 Ma (10)
241-243 Ma (2)
Guoluolongwa
Kedenongshe
403 Ma (3)
Delong
433-472 Ma (4)
256Ma (5)
454Ma (6)
0
5km
N
Quaternary system
Early-Middle Triassic strata
Late Permian stata
Carboniferous-Middle Permian strata
Late Devonian strata
Ordovician-Silurian Naij Tai group
Proterozoic metamorphic rocks
Late Permian-Triassic granitoid
Devonian syenogranite
Ordovician granitoid
Ophiolite
fault
gold deposit
454Ma
Zircon U-Pb ages

Fig. 3

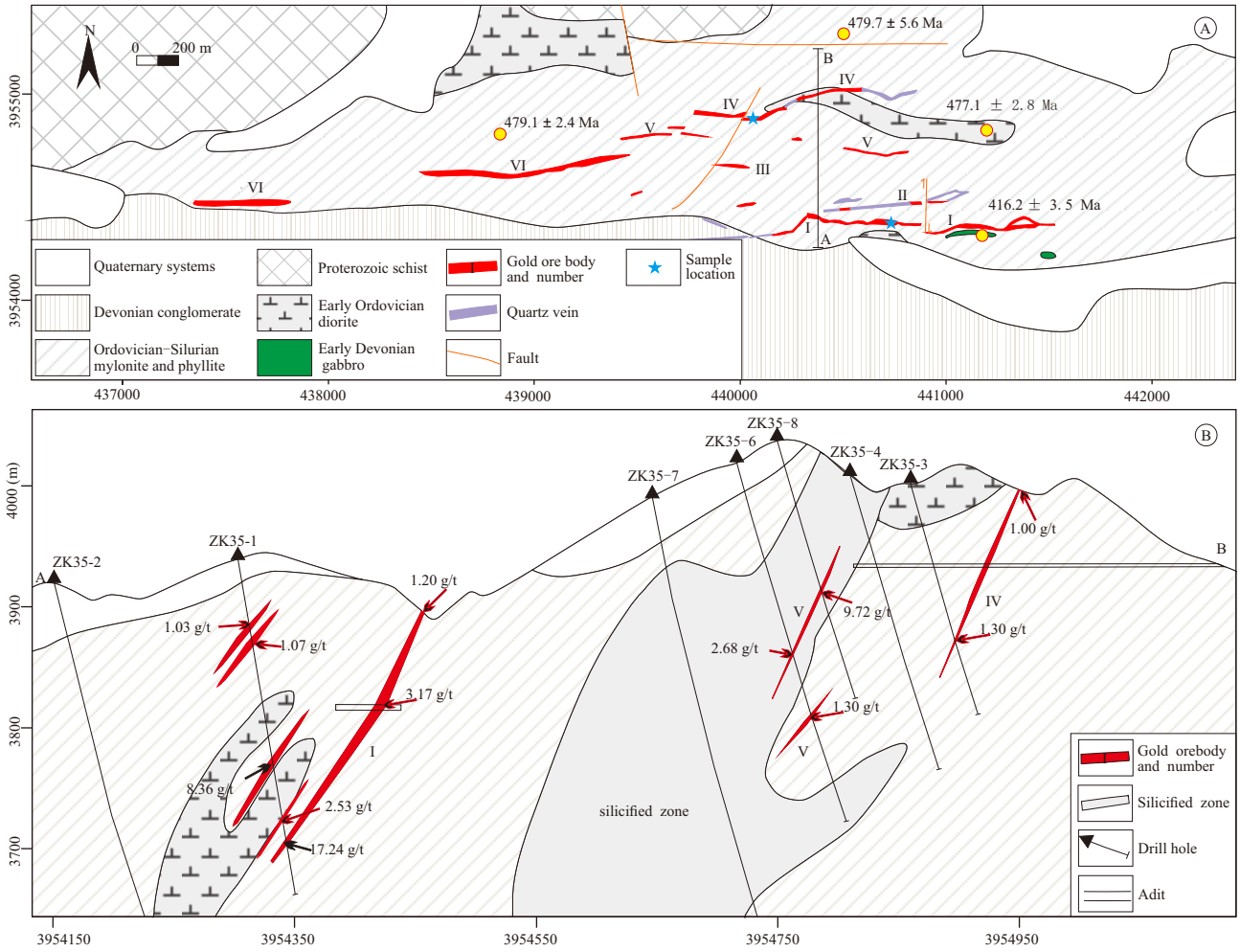
N
0 200 m
479.7 ± 5.6 Ma
479.1 ± 2.4 Ma
477.1 ± 2.8 Ma
416.2 ± 3.5 Ma
A
B
I
II
III
IV
V
VI
Quaternary systems
Devonian conglomerate
Ordovician–Silurian mylonite and phyllite
Proterozoic schist
Early Ordovician diorite
Early Devonian gabbro
Gold ore body and number
Quartz vein
Fault
Sample location
3955000
3954000
437000
438000
439000
440000
441000
442000
4000 (m)
3900
3800
3700
ZK35-1
ZK35-2
ZK35-3
ZK35-4
ZK35-6
ZK35-7
ZK35-8
1.03 g/t
1.07 g/t
1.20 g/t
3.17 g/t
8.36 g/t
2.53 g/t
17.24 g/t
2.68 g/t
9.72 g/t
1.30 g/t
1.00 g/t
1.30 g/t
silicified zone
Gold orebody and number
Silicified zone
Drill hole
Adit
3954150
3954350
3954550
3954750
3954950

Fig. 4

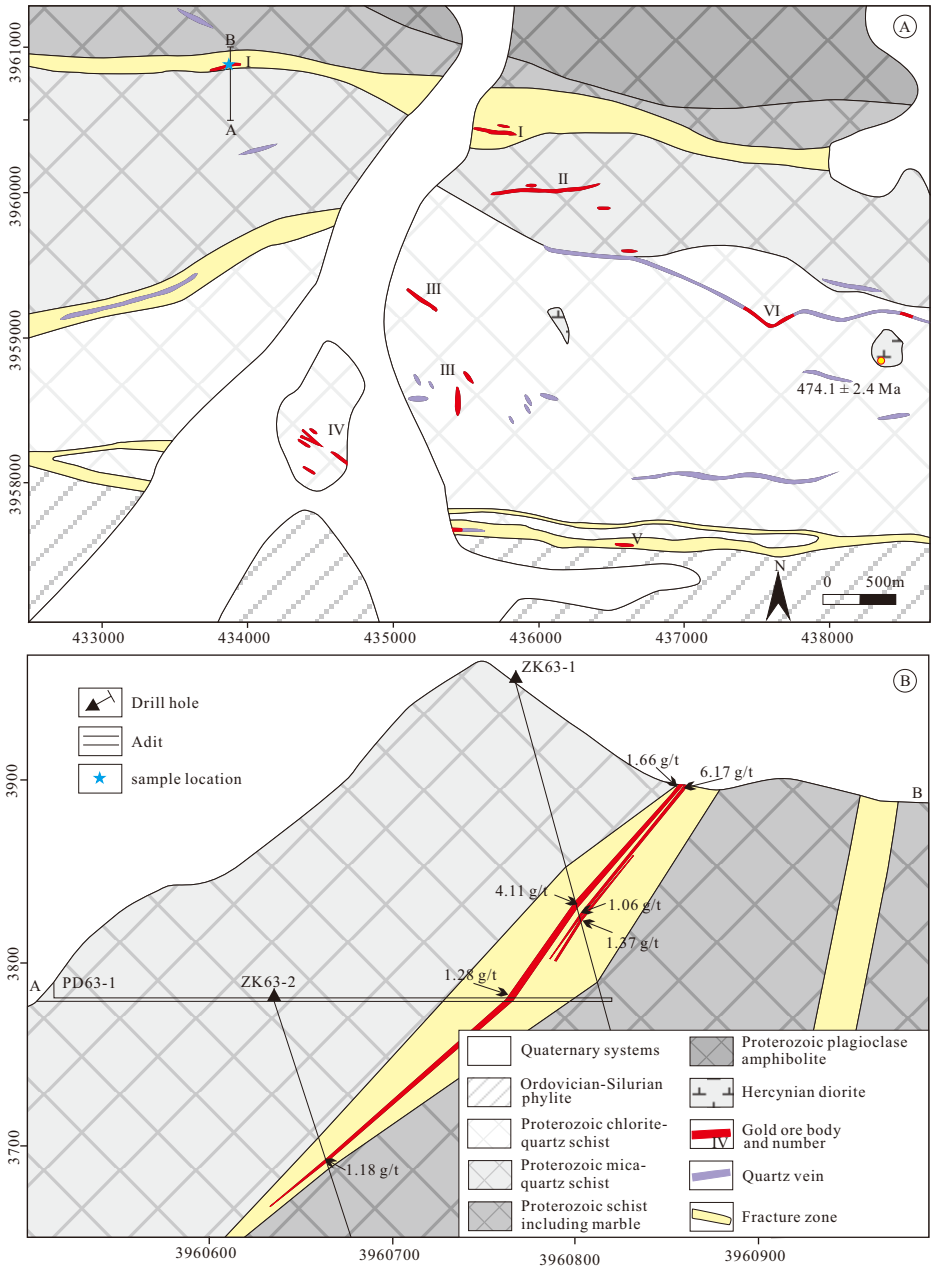
A
B
I
A
II
III
III
IV
V
VI
474.1 ± 2.4 Ma
N
0
500m
3961000
3960000
3959000
3958000
433000
434000
435000
436000
437000
438000
B
ZK63-1
Drill hole
Adit
sample location
1.66 g/t
6.17 g/t
B
4.11 g/t
1.06 g/t
1.37 g/t
1.28 g/t
A
PD63-1
ZK63-2
1.18 g/t
3900
3800
3700
3960600
3960700
3960800
3960900
Quaternary systems
Ordovician-Silurian phylite
Proterozoic chlorite-quartz schist
Proterozoic mica-quartz schist
Proterozoic schist including marble
Proterozoic plagioclase amphibolite
Hercynian diorite
Gold ore body and number
Quartz vein
Fracture zone

Fig. 5

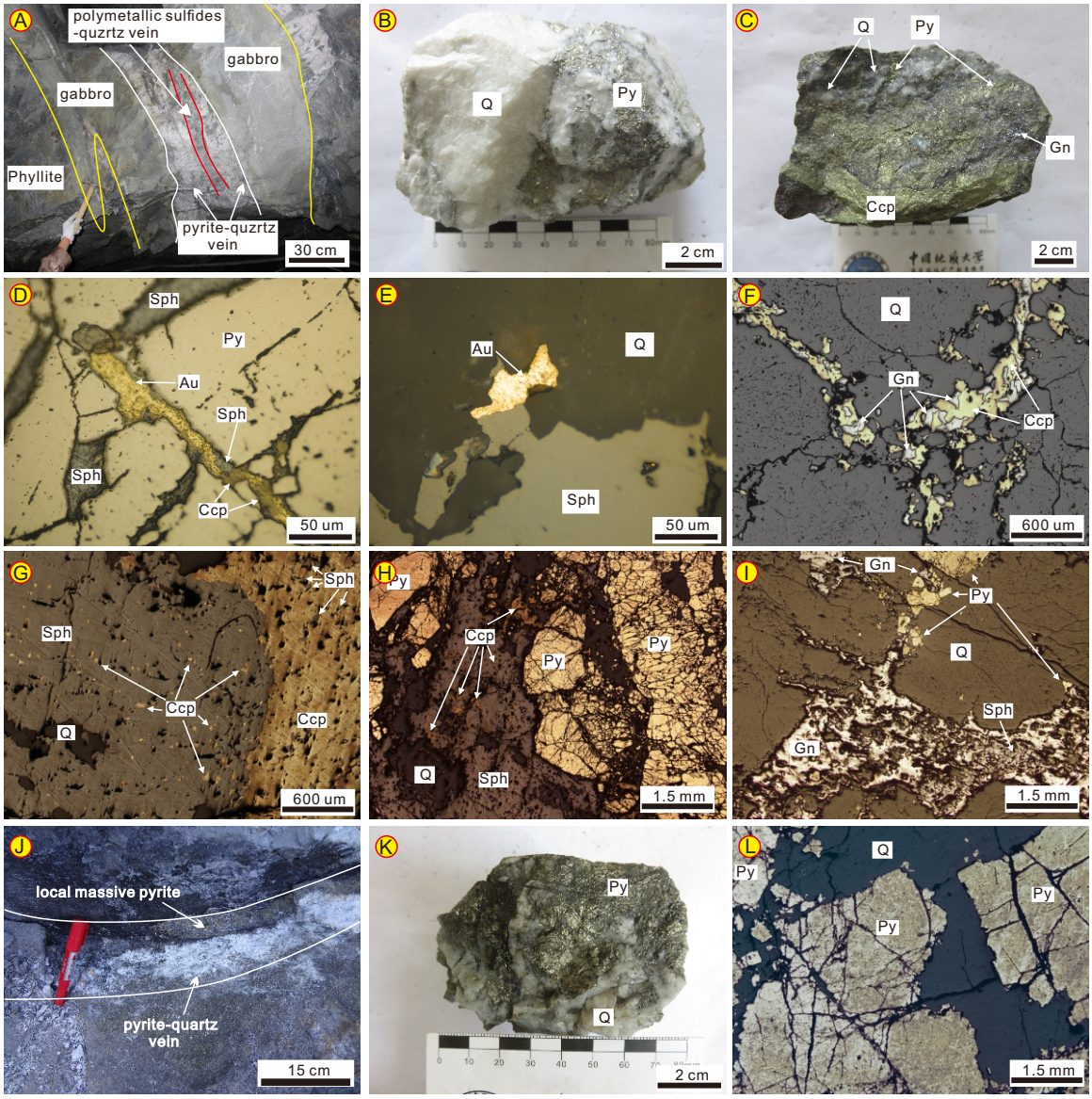
A
polymetallic sulfides
-quzrtz vein
gabbro
gabbro
Phyllite
pyrite-quzrtz
vein
30 cm
B
Q
Py
2 cm
C
Q
Py
Gn
Ccp
2 cm
D
Sph
Py
Au
Sph
Sph
Ccp
50 um
E
Au
Q
Sph
50 um
F
Q
Gn
Ccp
600 um
G
Sph
Sph
Ccp
Ccp
Q
600 um
H
Py
Ccp
Py
Py
Q
Sph
1.5 mm
I
Gn
Py
Q
Sph
Gn
1.5 mm
J
local massive pyrite
pyrite-quartz
vein
15 cm
K
Py
Q
2 cm
L
Q
Py
Py
Py
Py
1.5 mm

Fig. 6

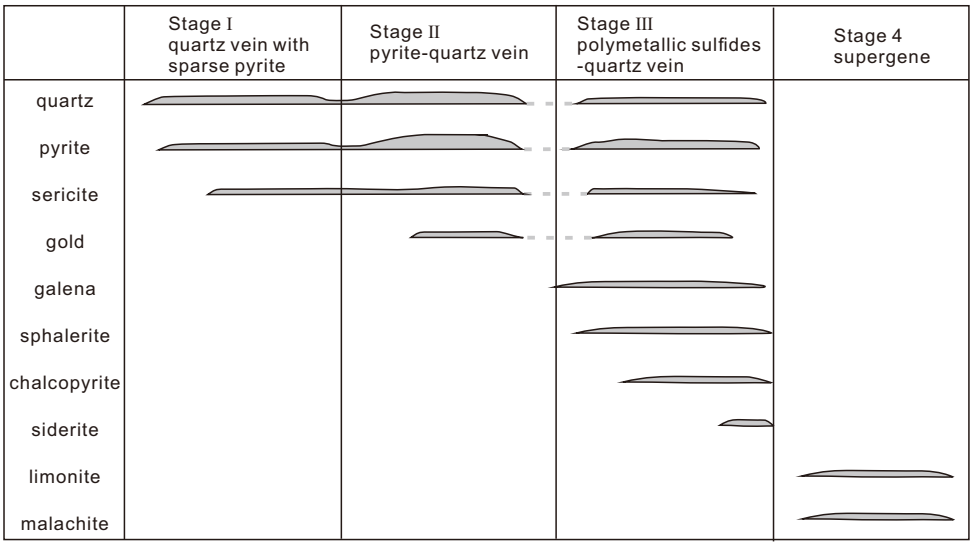
Stage I
quartz vein with
sparse pyrite
Stage II
pyrite-quartz vein
Stage III
polymetallic sulfides
-quartz vein
Stage 4
supergene
quartz
pyrite
sericite
gold
galena
sphalerite
chalcopyrite
siderite
limonite
malachite

Fig. 7

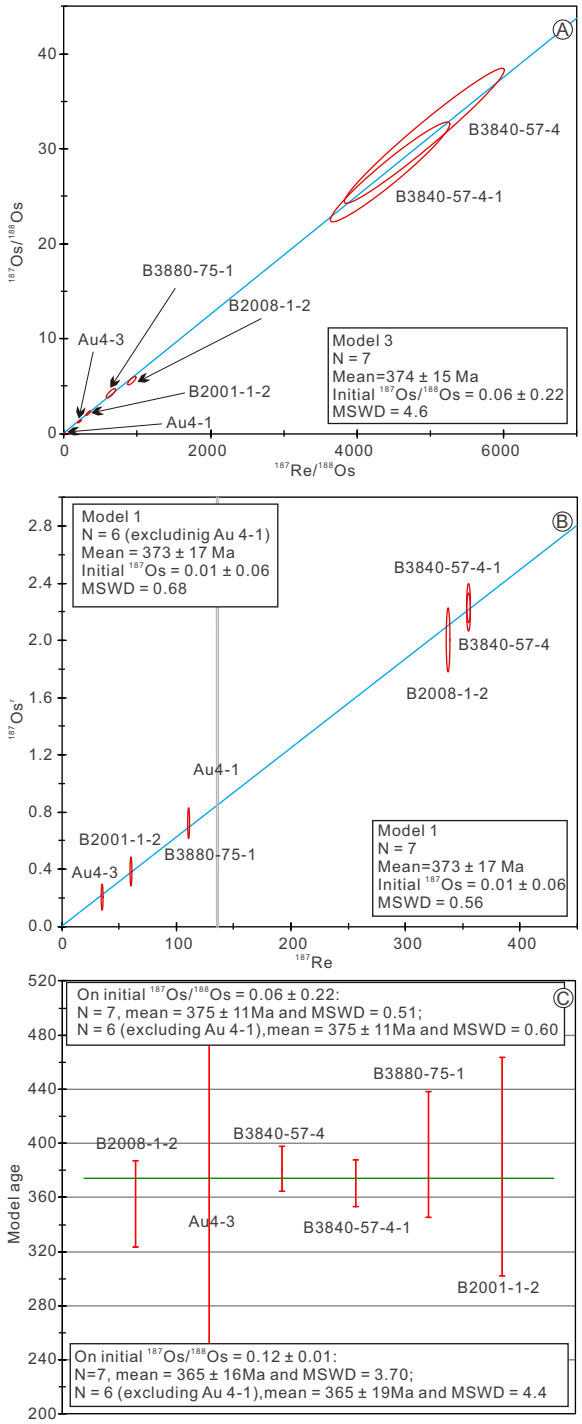
A
B3840-57-4
B3840-57-4-1
B3880-75-1
B2008-1-2
Au4-3
B2001-1-2
Au4-1
Model 3
N = 7
Mean=374 ± 15 Ma
Initial 187Os/188Os = 0.06 ± 0.22
MSWD = 4.6
187Os/188Os
187Re/188Os
B
Model 1
N = 6 (excludinig Au 4-1)
Mean = 373 ± 17 Ma
Initial 187Os = 0.01 ± 0.06
MSWD = 0.68
B3840-57-4-1
B3840-57-4
B2008-1-2
Au4-1
B2001-1-2
B3880-75-1
Au4-3
Model 1
N = 7
Mean=373 ± 17 Ma
Initial 187Os = 0.01 ± 0.06
MSWD = 0.56
187Os*
187Re
C
On initial 187Os/188Os = 0.06 ± 0.22:
N = 7, mean = 375 ± 11Ma and MSWD = 0.51;
N = 6 (excluding Au 4-1),mean = 375 ± 11Ma and MSWD = 0.60
B3880-75-1
B2008-1-2
B3840-57-4
Au4-3
B3840-57-4-1
B2001-1-2
Model age
On initial 187Os/188Os = 0.12 ± 0.01:
N=7, mean = 365 ± 16Ma and MSWD = 3.70;
N = 6 (excluding Au 4-1),mean = 365 ± 19Ma and MSWD = 4.4

Fig. 8

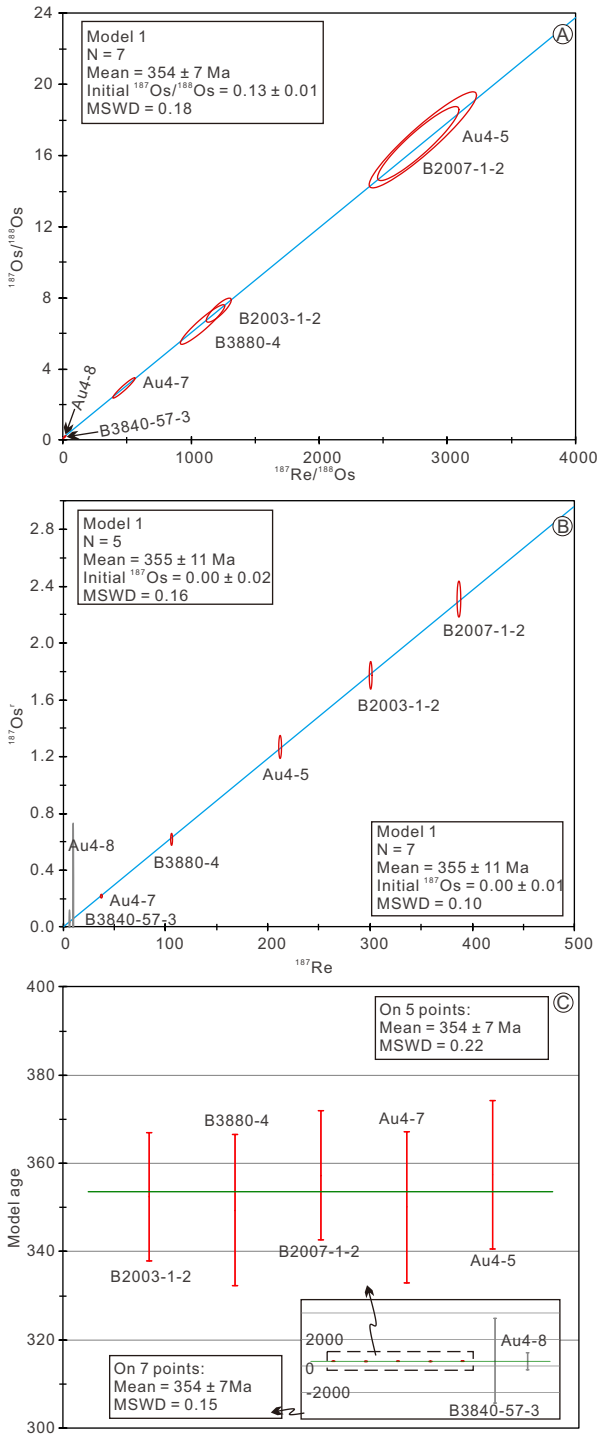
Model 1
N = 7
Mean = 354 ± 7 Ma
Initial 187Os/188Os = 0.13 ± 0.01
MSWD = 0.18
A
Au4-5
B2007-1-2
B2003-1-2
B3880-4
Au4-7
Au4-8
B3840-57-3
187Os/188Os
187Re/188Os
Model 1
N = 5
Mean = 355 ± 11 Ma
Initial 187Os = 0.00 ± 0.02
MSWD = 0.16
B
B2007-1-2
B2003-1-2
Au4-5
Au4-8
B3880-4
Au4-7
B3840-57-3
Model 1
N = 7
Mean = 355 ± 11 Ma
Initial 187Os = 0.00 ± 0.01
MSWD = 0.10
187Os*
187Re
On 5 points:
Mean = 354 ± 7 Ma
MSWD = 0.22
C
B3880-4
Au4-7
B2003-1-2
B2007-1-2
Au4-5
Model age
On 7 points:
Mean = 354 ± 7Ma
MSWD = 0.15
2000
0
-2000
Au4-8
B3840-57-3

Fig. 9

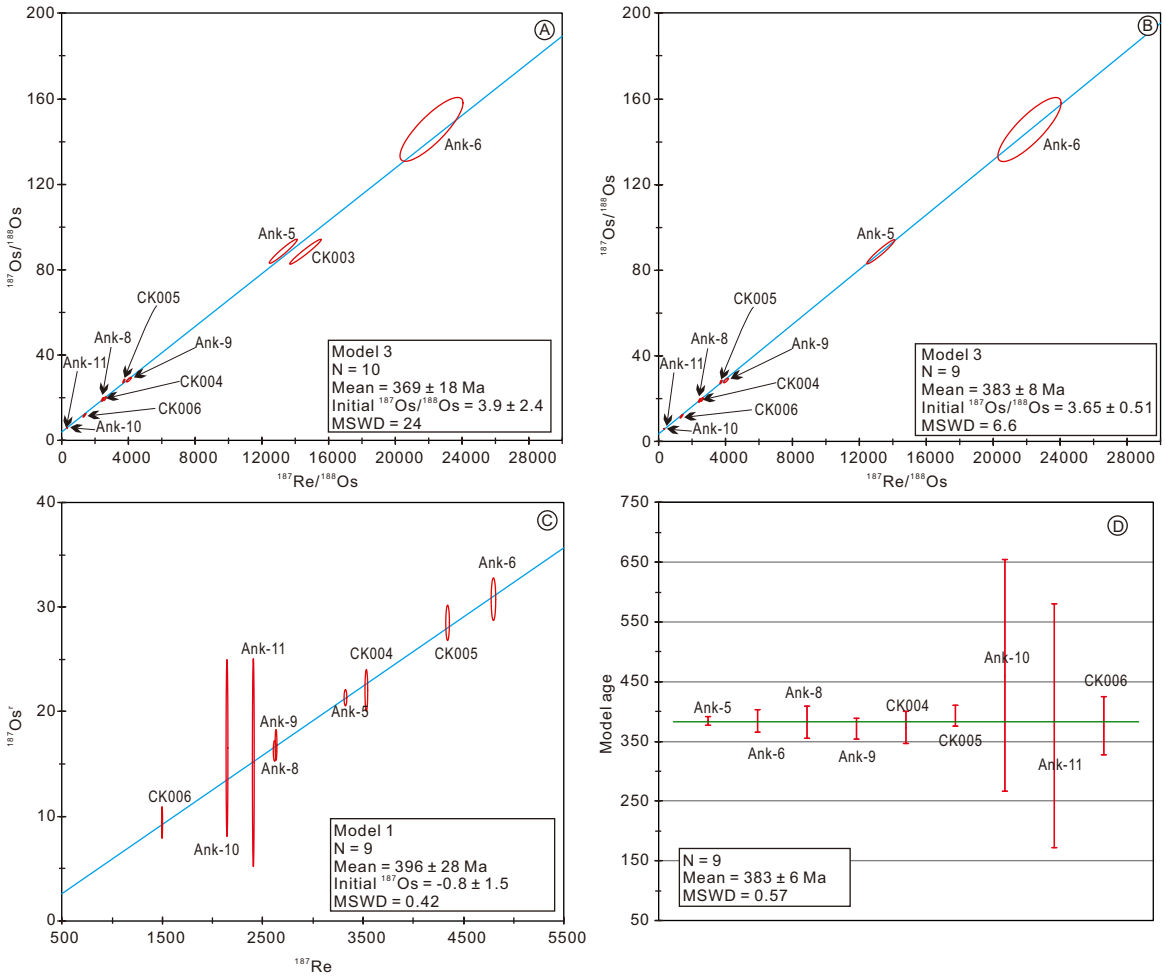
A
Ank-6
Ank-5
CK003
CK005
Ank-8
Ank-9
Ank-11
CK004
CK006
Ank-10
Model 3
N = 10
Mean = 369 ± 18 Ma
Initial 187Os/188Os = 3.9 ± 2.4
MSWD = 24
187Os/188Os
187Re/188Os
B
Model 3
N = 9
Mean = 383 ± 8 Ma
Initial 187Os/189Os = 3.65 ± 0.51
MSWD = 6.6
C
187Os*
Model 1
N = 9
Mean = 396 ± 28 Ma
Initial 187Os = -0.8 ± 1.5
MSWD = 0.42
187Re
D
Model age
N = 9
Mean = 383 ± 6 Ma
MSWD = 0.57

Fig. 10

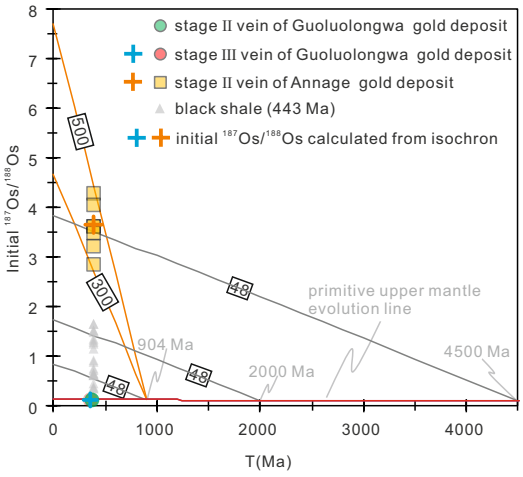
stage II vein of Guoluolongwa gold deposit
stage III vein of Guoluolongwa gold deposit
stage II vein of Annage gold deposit
black shale (443 Ma)
initial 187Os/188Os calculated from isochron
500
300
48
primitive upper mantle
evolution line
904 Ma
2000 Ma
4500 Ma
Initial 187Os/188Os
T(Ma)
0
1000
2000
3000
4000
1
2
3
4
5
6
7
8

Fig. 11

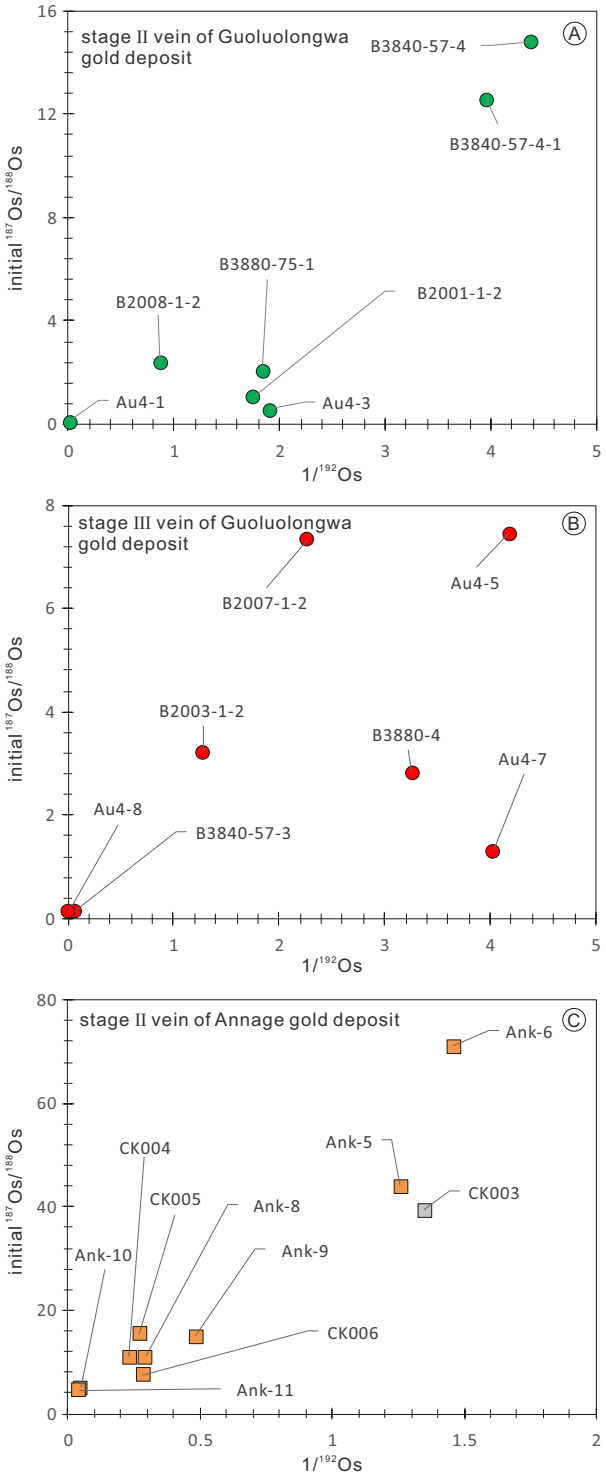
stage II vein of Guoluolongwa gold deposit
A
B3840-57-4
B3840-57-4-1
B3880-75-1
B2001-1-2
B2008-1-2
Au4-1
Au4-3
initial $^{187}Os/^{188}Os$
$1/^{192}Os$
stage III vein of Guoluolongwa gold deposit
B
B2007-1-2
Au4-5
B2003-1-2
B3880-4
Au4-7
Au4-8
B3840-57-3
initial $^{187}Os/^{188}Os$
$1/^{192}Os$
stage II vein of Annage gold deposit
C
Ank-6
CK004
Ank-5
CK005
Ank-8
CK003
Ank-10
Ank-9
CK006
Ank-11
initial $^{187}Os/^{188}Os$
$1/^{192}Os$

Fig. 12

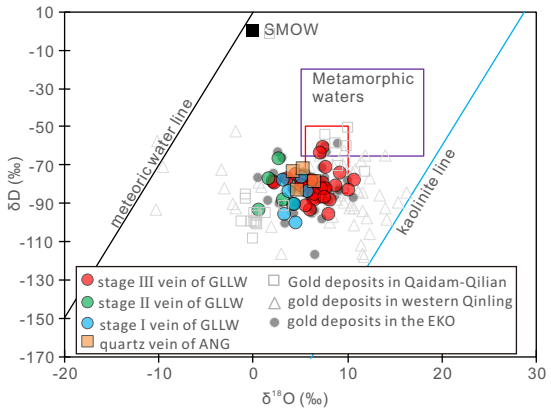
SMOW
Metamorphic waters
meteoric water line
kaolinite line
δD (‰)
δ18O (‰)
10
-10
-30
-50
-70
-90
-110
-130
-150
-170
-20
-10
0
10
20
30
stage III vein of GLLW
stage II vein of GLLW
stage I vein of GLLW
quartz vein of ANG
Gold deposits in Qaidam-Qilian
gold deposits in western Qinling
gold deposits in the EKO

Fig. 13

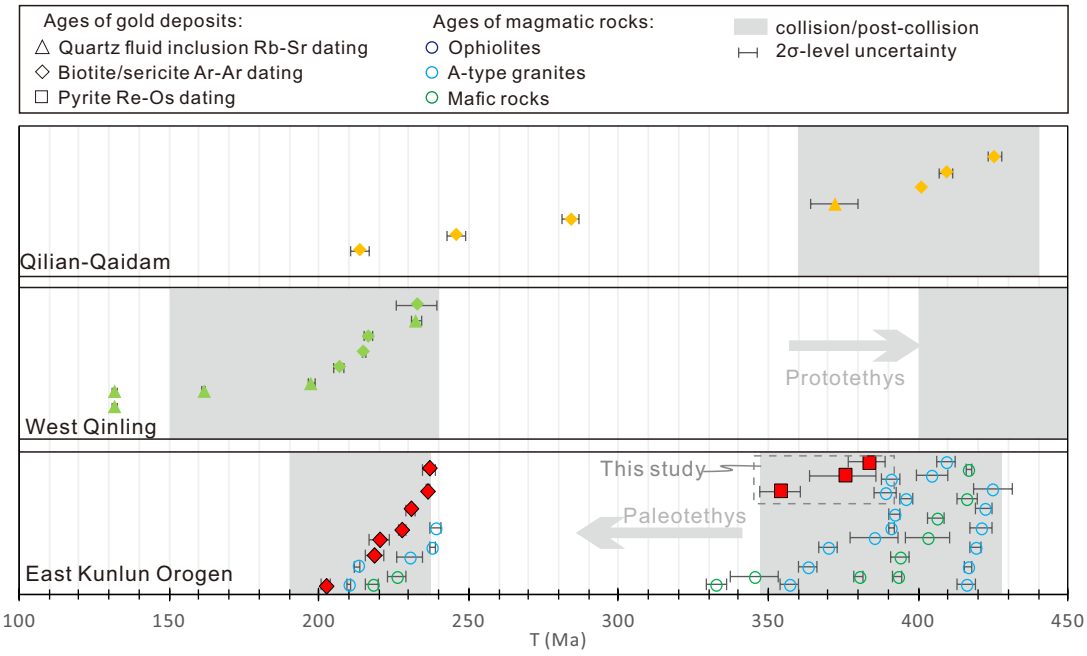
Ages of gold deposits:
Quartz fluid inclusion Rb-Sr dating
Biotite/sericite Ar-Ar dating
Pyrite Re-Os dating
Ages of magmatic rocks:
Ophiolites
A-type granites
Mafic rocks
collision/post-collision
2σ-level uncertainty
Qilian-Qaidam
West Qinling
East Kunlun Orogen
Prototethys
Paleotethys
This study
100
150
200
250
300
350
400
450
T (Ma)

Appendix table A1 Typical gold deposits in the west of the Central Orogenic Belt of China

deposit	resources (t)	Tectonic terrain	mineralization age (Ma)	mineral and method	reference
Hanshan		Qilian	372 ± 8; 213.9 ± 3.1	Quartz, Rb-Sr; Sericite, K-Ar	(Mao et al., 2000; Yang et al., 2005)
Yeluotuoquan		Qaidam	246 ± 3	Sericite, Ar-Ar	(Zhang et al., 2005)
Tanjianshan		Qaidam	284 ± 3; 401	Sericite and biotite, Ar-Ar;	(Zhang et al., 2005)
Qinglonggou		Qaidam	409.4 ± 2.3	Sericite, Ar-Ar	(Zhang et al., 2005)
Saibagou		Qaidam	425.5 ± 2.1	Sericite, Ar-Ar	(Zhang et al., 2005)
Wulonggou	72.93	East Kunlun Orogen	236.5 ± 0.5	Sericite, Ar-Ar	(Zhang et al., 2005)
Shuizhadonggou Huanglonggou	45.00	East Kunlun Orogen	230.8 ± 1.7; 237 ± 2	Sericite, Ar-Ar	(Zhang et al., 2017)
Guoluolongwa	40.00	East Kunlun Orogen	202.7 ± 1.5	Sericite, Ar-Ar	(Xiao et al., 2014)
Dachang	220.00	East Kunlun Orogen	218.6 ± 3.2; 220.3 ± 3.2	Sericite, Ar-Ar	(Feng, 2002; Zhang et al., 2005)
Naomuhun		East Kunlun Orogen	227.84 ± 1.13	Sericite, Ar-Ar	(Li et al., 2017)
Guoluolongwa	40.00	East Kunlun Orogen	202.7 ± 1.5; 375 ± 11; 354±7	Pyrite, Re-Os	(Xiao et al., 2014; This study)
Annage		East Kunlun Orogen	383 ± 6	Pyrite, Re-Os	This study
Baguamiao	106.00	western Qinling	232.58 ± 1.59; 131.9 ± 0.98; 131.91 ± 0.89	Quartz, Ar–Ar	(Shao andWang, 2001)
Xiaogouli		western Qinling	197.45 ± 1.13	Quartz, Ar–Ar	(Shao andWang, 2001)
Shangjiagou		western Qinling	161.59 ± 0.56	Quartz, Ar–Ar	(Shao andWang, 2001)
Liziyuan		western Qinling	206.8 ± 1.6	Sericite, K–Ar	(Liu et al., 2011)
Liba	80.00	western Qinling	216.4 ± 1.5	Muscovite and biotite, Ar–Ar	(Zeng et al., 2012)
Huachanggou	10.00	western Qinling	215 ± 0.5	Fuchsite, K–Ar	(Bai, 1996)

Jinlongshan	>150	western Qinling	232.7 ± 6.9	Sericite, Ar–Ar	(Zhao et al., 2001)
Yangshan	>300	western Qinling	197.6 ± 1.7	Zircon, U-Pb (SHRIMP)	(Qi et al., 2005)

Appendix table A2 A-type granites and related mafic rocks in the East Kunlun Orogen

Location	**lithology**	**age (Ma)**	**method**	**references**
Yugouzi	A-type granite	210 ± 0.6	Zircon LA-ICPMS U-Pb	(Gao, 2013)
Yemaquan	A-type granite	213 ± 1	Zircon LA-ICPMS U-Pb	(Gao et al., 2014)
Kendekeke	A-type granite	230.5 ± 4.2	Zircon LA-ICPMS U-Pb	(Xi et al., 2010)
Baishiya	A-type granite	238 ± 1	Zircon LA-ICPMS U-Pb	(Yin et al., 2013)
Halashan	A-type granite	239.2 ± 1.7	Zircon LA-ICPMS U-Pb	(He, 2015)
Tula	A-type granite	385.2 ± 8.1	Zircon SHRIMP U-Pb	(Wu et al., 2007)
Wulanwuzhuer	A-type granite	388.9 ± 3.7	Zircon LA-ICPMS U-Pb	(Guo et al., 2011)
Binggou	A-type granite	391 ± 3	Zircon LA-ICPMS U-Pb	(Liu et al., 2013)
Xiarihamu	A-type granite	391 ± 1	Zircon LA-ICPMS U-Pb	(Wang et al., 2013)
Dagangou	A-type granite	392 ± 2	Zircon LA-ICPMS U-Pb	(Tian et al., 2016)
Lalingzaohuo	A-type granite	396 ± 2	Zircon LA-ICPMS U-Pb	(Chen et al., 2013)
Shuizhadonggou	A-type granite	404.6 ± 5.2	Zircon LA-ICPMS U-Pb	(Wang, 2015)
Shuizhadonggou	A-type granite	409.3 ± 2.8	Zircon LA-ICPMS U-Pb	(Wang, 2015)
Dacaigou	A-type granite	416 ± 3	Zircon LA-ICPMS U-Pb	(Wang, 2015)
Huanglonggou	A-type granite	416.9 ± 1.3	Zircon LA-ICPMS U-Pb	(Li et al., 2014)
Houtougou	A-type granite	419 ± 1.9	Zircon LA-ICPMS U-Pb	(Yan et al., 2016)
Baiganhu	A-type granite	421 ± 3.7	Zircon SHRIMP U-Pb	(Li et al., 2012)
Baiganhu	A-type granite	422 ± 3	Zircon SHRIMP U-Pb	(Li et al., 2012)
Helegangnaren	A-type granite	425 ± 6.7	Zircon LA-ICPMS U-Pb	(Li et al., 2013)
Zongjia	basic dike	218±2	Zircon LA-ICPMS U-Pb	(Xiong, 2014)

Binggou	basic dike	226±3	Zircon LA-ICPMS U-Pb	(Xiong, 2014)
Qimantage	dolerite	380.3 ± 1.5	Zircon LA-ICPMS U-Pb	(Qi et al., 2013)
East of Yuejinshan	hornblende gabbro	393.1 ± 1.6	Zircon LA-ICPMS U-Pb	(Xiong et al., 2014)
Xiarihamu	gabbro	394 ± 3	Zircon LA-ICPMS U-Pb	(Li et al., 2012)
Geyakedengtage	gabbro	403.3 ± 7.2	Zircon SHRIMP U-Pb	(Chen et al., 2006)
Yuejinshan	gabbro	406 ± 3	Zircon LA-ICPMS U-Pb	(Liu et al., 2012)
Guoluolongwa	lamprophyre	416.3 ± 3.5	Zircon LA-ICPMS U-Pb	(Yue et al., 2013)
Sederi	dolerite	417 ± 1	Zircon LA-ICPMS U-Pb	(Yue et al., 2017)
Haerguole	gabbro from ophiolite	332.8 ± 3.1	Zircon LA-ICPMS U-Pb	(Liu et al., 2011)
Xiadawu	gabbro from ophiolite	345.3 ± 7.9	whole rock Ar-Ar	(Chen et al., 2001)

REFERENCES

Chen, L., Sun, Y., Pei, X.Z., Gao, M., Tao, F., Zhang, Z.Q., Chen, W., 2001, Northernmost Paleo-Tethyan oceanic basin in Tibet: geochronological evidence from 40Ar/39Ar age dating of Dur'ngoi ophiolite: Chinese Science Bulletin, v. 46, p. 1203-1205.

Li, R.B., Pei, X.Z., Li, Z.C., Sun, Y., Pei, L., Chen, G.C., Chen, Y.X., Liu, C.J., Wei, F.H., 2013, Regional tectonic transformation in East Kunlun Orogenic Belt in Early Paleozoic: constraints from the geochronology and geochemistry of Helegangnaren alkali-feldspar granite: Acta Geologica Sinica, v. 87, p. 333-345.

Xiong, F.H., Ma, C.Q., Jiang, H.A., Liu, B., Huang, J., 2014, Geochronology and geochemistry of Middle Devonian mafic dykes in the East

Kunlun orogenic belt, Northern Tibet Plateau: Implications for the transition from Prototethys to Paleotethys orogeny: Chemie der Erde - Geochemistry, v. 74, p. 225-235.

Zeng, Q.T., McCuaig, T.C., Hart, C.J.R., Jourdan, F., Muhling, J., Bagas, L., 2012, Structural and geochronological studies on the Liba goldfield of the West Qinling Orogen, Central China: Mineralium Deposita, v. 47, p. 799-819.

Zhang, J.Y., Ma, C.Q., Li, J.W., Pan, Y.M., 2017, A possible genetic relationship between orogenic gold mineralization and post-collisional magmatism in the eastern Kunlun Orogen, western China: Ore Geology Reviews, v. 81, Part 1, p. 342-357.

Bai, Z., 1996, Genesis of the Huachanggou gold deposit in Shanxi Province: Mineral Resources and Geology, v. 10, p. 108-113 (in Chinese with English abs.).

Chen, J., Xie, Z.Y., Li, B., Tan, S.X., Ren, H., Zhang, Q.M., Li, Y., 2013, Petrogenesis of Devonian intrusive rocks in Lalingzaohuo area, Eastern Kunlun, and its geological significance: Journal of Mineralogy and Petrology, v. 33, p. 26-34 (in Chinese with English abs.).

Chen, H.W., Luo, Z.H., Mo, X.X., Zhang, X.T., Wang, J., Wang, B.Z., 2006, SHRIMP ages of Kayakedengtage complex in the East Kunlun Mountains and their geological implications: Acta Petrologica Et Mineralogica, v. 25, p. 25-32 (in Chinese with English abs.).

Feng, C.Y., 2002, Multiple orogenic processes and mineralization of orogenic gold deposits in the East Kunlun Orogen, Qinghai province: Ph.D.

thesis, Beijing, Chinese Academy of Geological Sciences, 104p (in Chinese with English abs.).

Gao, Y.B., 2013, The intermediate-acid intrusive magmatism and mineralization in Oimantag, East Kunlun Mountains: Ph.D. thesis, Xi'an, Chang'an University, 1-245p (in Chinese with English abs.).

Gao, Y.B., Li, W.Y., Qian, B., Li, K., Li, D.S., He, S.Y., Zhang, Z.W., Zhang, J.W., 2014, Geochronology, geochemistry and Hf isotopic compositions of the granitic rocks related with iron mineralization in Yemaquan deposit, East Kunlun, NW China: Acta Petrologica Sinica, v. 30, p. 1647-1665 (in Chinese with English abs.).

Guo, T.Z., Liu, R., Chen, F.B., Bai, X.D., Li, H.G., 2011, LA-MC-ICPMS zircon U-Pb dating of Wulanwuzhuer porphyritic syenite granite in the Qimantag Mountain of Qinghai and its geological significance: Geological Bulletin of China, v. 30, p. 1203-1211 (in Chinese with English abs.).

He, C., 2015, Geological characteristics，genesis and geological significance of granite intrusion in Halasen area，Qinghai Province: master thesis, Wuhan, China University of Geosciences (Wuhan), 1-46p (in Chinese with English abs.).

Li, G.C., Feng, C.Y., Wang, R.J., Ma, S.C., Li, H.M., Zhou, A.S., 2012, SIMS zircon U-Pb age, petrochemistry and tectonic implications of granitoids in northeastern Baiganhu W-Sn orefield, Xinjiang: Acta Geoscientica Sinica, v. 33, p. 216-226 (in Chinese with English abs.).

Li, J.C., Kong, H.L., Su, Y.Z., Namkha, N., Jia, Q.Z., Guo, X.Z., Zhang, B., 2017, Ar-Ar age of altered sericite, zircon U-Pb age of quartz diorite and geochemistry of the Naomuhun Gold deposit, East Kunlun: Acta Geologica Sinica, v. 91, p. 979-991 (in Chinese with English abs.).

Li, S.J., Sun, F.Y., Gao, Y.W., Zhao, J.W., Li, L.S., Yang, Q.A., 2012, The theoretical guidance and the practice of small intrusions forming large deposits———The enlightenment and significance for searching breakthrough of Cu-Ni sulfide Deposit in Xiarihamu, East Kunlun, Qinghai: Northwestern Geology, v. 45, p. 185-191 (in Chinese with English abs.).

Li, X., Yuan, W.M., Hao, N.N., Duan, H.W., Chen, X.N., Mo, X.X., Zhang, A.K., 2014, Characteristics and tectonic setting of granite in Wulonggou area, East Kunlun Mountains: Global Geology, v. 33, p. 275-288 (in Chinese with English abs.).

Liu, B., Ma, C.Q., Guo, P., Zhang, J.Y., Xing, F.H., Huang, J., Jiang, H.A., 2013, Discovery of the Middle Devonian A-type granite from the Eastern Kunlun Orogen and its tectonic implications: Earth Science-Journal of China University of Geosciences, v. 38, p. 947-962 (in Chinese with English abs.).

Liu, B., Ma, C.Q., Zhang, J.Y., Xiong, F.H., Huang, J., Jiang, H.A., 2012, Petrogenesis of Early Devonian intrusive rocks in the east part of Eastern Kunlun Orogen and implication for Early Palaeozoic orogenic processes: Actor Petrologica Sinica, v. 28, p. 1785-1807 (in Chinese

with English abs.).

Liu, Y.H., Liu, H.L., Huang, S.F., Gao, H.X., Zhang, Y.Q., Li, Z.G., Zheng, X.Z., 2011, Metallogenic epoch and geological features of Suishizi porphyry gold deposit in Liziyuan area, west Qinling mountain: Gold, v. 32, p. 12-18 (in Chinese with English abs.).

Liu, Z.Q., Pei, X.Z., Li, R.B., Li, Z.C., Zhang, X.F., Liu, Z.G., Chen, G.C., Chen, Y.X., Ding, S.P., Guo, J.F., 2011, LA-ICP-MS zircon U-Pb geochronology of the two suites of ophiolites at the Buqingshan area of the A'nyemaqen Orogenic Belt in the southern margin of East Kunlun and its tectonic implication: Acta Geologica Sinica, v. 85, p. 185-194 (in Chinese with English abs.).

Mao, J.W., Zhang, Z.H., Yang, J.M., Wang, Z.L., 2000, Fluid inclusions of shear zone type gold deposits in the western part of North Qilian Mountain: Mineral Deposits, v. 19, p. 9-16 (in Chinese with English abs.).

Qi, J.Z., Li, L., Yuan, S.S., Liu, Z.J., Liu, D.Y., Wang, Y.B., Li, Z.H., 2005, A SHRIMP U-Pb chronological study of zircons from quartz veins of Yangshan gold deposit, Gansu Province: Mineral Deposits, v. 24, p. 141-150 (in Chinese with English abs.).

Qi, S.S., Deng, J.F., Ye, Z.F., Liu, R., Wang, G.L., 2013, LA-ICP-MS zircon U-Pb dating of Late Devonian diabase dike swarms in Qimantag area: Geological Bulletin of China, v. 32, p. 1385-1393 (in Chinese with English abs.).

Shao, S.C., Wang, D.B., 2001, 39Ar-40Ar dating of the three typical gold deposits and its geological significance in the southern Qinling region:

Acta Geologica Sinica, v. 75, p. 106-110 (in Chinese with English abs.).

Tian, G.K., Meng, F.C., Fan, Y.Z., Liu, Q., Duan, X.P., 2016, The characteristics of Early Paleozoic post-orogenic granite in the East Kunlun orogen: A case study of Dagangou granite: Acta Petrologica et Mineralogica, v. 35, p. 371-390 (in Chinese with English abs.).

Wang, G., Sun, F.Y., Li, B.Y., Li, S.J., Zhao, J.W., Yang, Q.A., Ao, Z., 2013, Zircon U-Pb geochronology and geochemistry of the Early Devonian syenogranite in the Xiarihamu ore district from East Kunlun, with Implications for the geodynamic setting: Geotectonica et Metallogenia, v. 37, p. 685-697 (in Chinese with English abs.).

Wang, T., 2015, Study of the geological characteristics and genesis of Wulonggou gold deposit, Qinghai province: master thesis, China University of Geosciences (Beijing), 84p (in Chinese with English abs.).

Wu, S.P., Wu, C.L., Chen, Q.L., 2007, Characteristics and tectonic setting of the Tula aluminous A-type granite at the south side of the Altyn Tagh fault, NW China: Geological Bulletin of China, v. 26, p. 1385-1392 (in Chinese with English abs.).

Xi, R.G., Xiao, P.X., Wu, Y.Z., Dong, Z.C., Guo, L., Gao, X.F., 2010, The geological significances, composition and age of the monzonitic granite in Kendekeke iron mine: Northwestern Geology, v. 43, p. 195-202 (in Chinese with English abs.).

Xiao, Y., Feng, C.Y., Li, D.X., Liu, J.N., 2014, Chronology and fluid inclusions of the Guoluolongwa gold deposit in Qinghai province: Acta

Geologica Sinica, v. 88, p. 895-902 (in Chinese with English abs.).

Xiong, F.H., 2014, Spatial-temporal pattern, petrogenesis and geological implications of Paleo-Tethyan granitoids in the East Kunlun Orogenic belt (eastern segment): Ph.D. thesis, Wuhan, China University of Geosciences, 1-191p (in Chinese with English abs.).

Yan, W., Qiu, D.M., Ding, Q.F., Liu, F., 2016, Geochronology, petrogenesis, source and its structural significance of Houtougou monzogranite of Wulonggou area in Eastern Kunlun Orogen: Journal of Jilin University (Earth Science Edition), v. 46, p. 443-460 (in Chinese with English abs.).

Yang, J.G., Yang, L.H., Ren, Y.X., Li, Z.P., Song, Z.B., 2005, Isotopic Geochronology of the ore-forming process in the Hanshan gold deposit of the North Qilian Mountains: Acta Geoscientica Sinica, v. 26, p. 315-320 (in Chinese with English abs.).

Yin, L.J., Liu, H.J., Yang, L.G., Liu, W.M., 2013, Geochronology, geochemistry and geological significance of granites from the Baishiya skarn iron-polymetallic deposit, Dulan, Qinghai Province: Xinjiang Geology, v. 31, p. 248-255 (in Chinese with English abs.).

Yue, W.H., Gao, J.G., Zhou, J.X., 2013, LA-ICP-MS Zircon U-Pb Ages and Lithogeochemistry of Basic Dykes in the Guoluolongwa gold ore Field, Qinghai Province, China: Journal of Mineralogy and Petrology, v. 33, p. 93-102 (in Chinese with English abs.).

Yue, W.H., Zhou, J.X., Gao, J.G., Huang, Y.H., Jia, F.J., 2017, Geochemistry，zircon U-Pb chronology and geological implications of Sederi

diabase，Dulan county，Qinghai province: Bulletin of Mineralogy，Petrology and Geochemistry, v. 36, p. 270-278 (in Chinese with English abs.).

Zhang, D.Q., Dang, X.Y., She, H.Q., Li, D.X., Feng, C.Y., Li, J.W., 2005, Ar-Ar dating of orogenic gold deposits in northern margin of Qaidam and East Kunlun Mountains and its geological significance: Mineral Deposits, v. 24, p. 87-98 (in Chinese with English abs.).

Zhao, L.Q., Chen, X., Zhou, H., Li, X.M., 2001, Metallogenic epoch of Jinlongshan micro-fine disseminated gold deposit, south Qinlin Mountain: Chinese Journal of Geology, v. 36, p. 489 (in Chinese with English abs.).